THE UNIVERSITY of ADELAIDE

Structure of the Kangaroo Island Fleurieu Peninsula Shear Zone and the Provenance of its host sediments- The Kanmantoo Group- South Eastern Australia

Amy Suto

Centre for Tectonic Resources and Exploration,

Department of Geology and Geophysics

School of Earth and Environmental Sciences,

University of Adelaide, South Australia

amy.suto@student.adelaide.edu.au

24th of October 2011

Contents

Structure of the Kangaroo Island Fleurieu Peninsula Shear Zone and the Provenance of its host sediments- The Kanmantoo Group- South Eastern Australia

Amy Suto

Centre for Tectonic Resources and Exploration,

Department of Geology and Geophysics

School of Earth and Environmental Sciences,

University of Adelaide, South Australia

amy.suto@student.adelaide.edu.au

ABSTRACT

The Kangaroo Island-Fleurieu Peninsula Shear Zone (KIFPSZ) is considered to be a major cratonic boundary which was active during the Delamerian Orogeny. As shear zones are extremely localized regions of high strain, they hold key spatial and temporal information about the tectonic evolution of a region, and thus, it is important to gain a complete understanding of their structure and dynamics. Detailed mapping and strain logs show that strain along the KIFPSZ varies in intensity and manifestation. Whilst mineral lineations and kinematics indicate north-west directed transport towards the Gawler Craton, foliations and bedding readings gradually rotated into more easterly orientation. At a microscopic scale, Electron Backscatter Diffraction (EBSD) analysis shows a variety of slip mechanisms across sampled sections that

also suggest an increase in intensity of deformation moving southwards. Strain logs and transect maps highlight lithological and spatial differences in strain manifestation, and show that the SAFTB was formed during subsequent compression against the angular, rigid, Gawler cratonic margin. U-Pb detrital zircon analysis on the Kanmantoo Group sedimentary rocks yielded maximum depositional ages of *ca* 620 – 590 Ma. Age spectra are dominated by Early Mesoproterozoic, Late Mesoproterozoic, Neoproterozoic and Late Neoproterozoic sources, constraining the source terrains of the Kanmantoo Trough to the Prydz-Leeuwin Belt, and the Gamburstev Subglacial Mountains. Results of this study provide a detailed structural analysis of the KIFPSZ; lend further support to the notion that the South Australian Fold-Thrust Belt was formed during the compression against an angular Gawler Craton and provide constraints on the source of sediments of the Kanmantoo Trough.

KEY WORDS

Kangaroo Island, Fleurieu Peninsula, Shear Zone, Kanmantoo, Provenance, South Australian Fold Thrust Belt (SAFTB), Detrital U-Pb, Zircon, Electron Backscatter Diffraction (EBSD), Crystallographic Preferred Orientation (CPO)

INTRODUCTION

Shear zones are important in reconstructing the tectonic evolution of the Earth's lithosphere. Shear zones are extremely localised regions of high strain and are often associated with crustal-scale boundaries. Therefore, they hold key spatial and temporal information about the tectonic

evolution of a region. Shear zone complexes can be dominated by pure shear, simple shear, or a combination of the two; which adds to the complexity of shear zone dynamics and the resulting geology. Microscopic or even macroscopic structures in one section of a shear zone may not be representative of the overall structural nature of the shear zone (Platt & Behrmann 1986; Klepeis *et al.* 1998; Weil *et al.* 2010). It is therefore important to gain a complete understanding of the strain history and dynamics of a shear zone before conclusions about tectonic evolution and, further, ancient continental reconstruction, can be inferred.

The Kangaroo Island- Fleurieu Peninsular Shear Zone (KIFPSZ), which forms part of the South Australian Fold Thrust Belt (SAFTB), is considered to be a long-lived tectonic boundary and crustal deformation zone (Flöttmann *et al.* 1995). The shear zone runs in an approximate east-west direction along Kangaroo Island into the Gulf of St Vincent, where it curves northwards and reappears on the mainland as a more north-east, south-west trending structure (Figure 1 and Figure 2). Structural analysis suggests that the KIFPSZ has accommodated a large degree of crustal compression and shortening during the Cambrian-Ordovician Delamerian Orogeny (Offler & Fleming 1968; von der Borch 1980; Fleming & White 1984; Coney *et al.* 1990; Sandiford *et al.* 1990; Dymoke & Sandiford 1992; Flöttmann *et al.* 1993; Powell *et al.* 1994; Flöttmann *et al.* 1995; Foden *et al.* 1999; Foden *et al.* 2006). During this event, Neoproterozoic to early Cambrian sequences of the Adelaidean, Normanville, Kanmantoo and Kangaroo Island Group sedimentary successions underwent contractional deformation developing a westward verging fold-thrust belt (Offler & Fleming 1968; Macktelow 1990; Jenkins & Sandiford 1992; Flöttmann *et al.* 1994; Foden *et al.* 2006). Previously, there has been mapping and analytical studies based on the geology of Kangaroo Island and the Fleurieu Peninsula, focusing on the

sedimentation, metamorphism and structural evolution of the SAFTB (Mancktelow 1981; Jenkins & Sandiford 1992; Belperio & Flint 1993; Flöttmann *et al.* 1994; Flöttmann *et al.* 1995; Flöttmann & Cockshell 1996; Marshak & Flöttmann 1996; Flo¨ttmann & James 1997; Flöttmann & James 1997; Yassaghi *et al.* 2000; Yassaghi *et al.* 2004; Direen *et al.* 2005; Fairclough 2008). A previous study by Marshak and Flöttmann (1996) offers a comparative analysis of nine shear zones and faults along the SAFTB on a regional scale that does not allow for detailed analysis of individual structures.

In order to understand the full strain history and dynamics of the KIFPSZ, and in turn, increase the understanding of the SAFTB and Delamerian Orogeny, this study presents a detailed analysis using strain logs, and field mapping along the shear zone. Electron Backscatter Diffraction (EBSD) data has been obtained to observe the preferred crystallographic orientation of quartz grains from within the shear zone, which can be used to determine intra-crystalline slip systems active during deformation that can help determine the temperature of deformation (Pauli *et al.* 1996; Passchier & Trouw 2005; Toy *et al.* 2008), assist in kinematic analysis (Schmid & Casey 1986; Schmidt & Olesen 1989; Passchier & Trouw 2005) and help reveal strain partitioning within a rock. To further understand the provenance of the Kanmantoo Group sediments involved in the shear zone, U-Pb zircon laser inductively-coupled plasma mass spectrometry (LA-ICPMS) geochronology was undertaken on three samples. These techniques therefore provide a comprehensive and relevant dataset that; 1) Allows for further understanding of the structure and strain dynamics in the KIFPSZ; 2) Helps constrain the provenance of the Kanmantoo Group and; 3) Adds to the understanding of the formation and deformation of the SAFTB, and its significance in ancient continental reconstructions.

BACKGROUND

Geological Frame Work

The South Australian Fold Thrust Belt (SAFTB) records multiple stages of rifting, sedimentation and deformation spanning nearly 450 million years from approximately 800 Ma to 490 Ma (Powell *et al.* 1994; Preiss 2000). It can be subdivided into three distinct zones: the Nackara Arc; the Transitional Domain and the Fleurieu Arc (Figure 1b; Marshak & Flöttmann 1996). The KIFPSZ forms part of the Fleurieu Arc, which represents the southern-most extension of the SAFTB. The north-east striking, south dipping KIFPSZ is considered to be a fundamental detachment zone and a major cratonic boundary (Flöttmann *et al.* 1993; Flöttmann *et al.* 1995), as it forms the northernmost boundary of the extensive Kanmantoo Group on Kangaroo Island and thrusted Paleoproterozoic (Hand *et al.* 2007) basement over Adelaidian Rift Complex rocks on the Fleurieu Peninsula during the middle to late Cambrian Delamerian Orogeny. The Delamerian Orogeny is constrained to between 514 ±3 Ma and 490 ±3 Ma (Foden *et al.* 2006) and is characterised by low pressure, high temperature metamorphism (Offler & Fleming 1968; Macktelow 1990; Sandiford *et al.* 1990; Sandiford *et al.* 1992) with mineral assemblages that indicate peak metamorphism occurred at approximately 3-4 kbars and 650°C (Sandiford *et al.* 1990; Sandiford *et al.* 1992). Convergence during the Cambrian was initiated in the south (Antarctica) and propagated northward (Flöttmann *et al.* 1998) resulting in the deformation with tight folding and west-directed structures.

Stratigraphy

ADELAIDEAN BASIN

Deposition of the Adelaidean Basin Rift Complex reflects a protracted period of basin formation, which is thought to have been attributed to lithospheric attenuation commencing around 800 Ma (U-Pb zircon age of 802±2 Ma from the Callana beds (Preiss 2000)). The Adelaidean Rift Complex has been divided into three supergroups; the Warrina Supergroup, the Heysen Supergroup and the Moralana Supergroup. The Warrina Supergroup encompasses the early-rift sequences of the Callana and Burra groups, while the Heysen Supergroup consists of the glacial, interglacial and post-glacial Umberatana and Wilpena Groups (Preiss 2000). The southern Fleurieu Peninsula is dominated by the Callana and Burra groups (Figure 3).

KANMANTOO GROUP

The Kanmantoo Group which is exposed in the southern part of the Fleurieu Arc was deposited in the short-lived and localised Kanmantoo Trough (Figure 1b). The Kanmantoo Trough represents a major change in the depositional history in the SAFTB from a rift basin to a foreland basin (Fig. 3; Daily & Milnes 1973; Daily *et al.* 1979; Gatehouse *et al.* 1990; Gravestock & Gatehouse 1995; Jago *et al.* 2003). At the time of its deposition, the Kanmantoo Trough was thought to be situated close to the eastern (Paleo-Pacific) continental margin of Gondwana (Figure 1a; Flöttmann *et al.* 1993; Flöttmann *et al.* 1998). The true thickness of the Kanmantoo Group is estimated at 7-8 km and the sedimentary package as a whole is thought to represent a

shallow water, slope environment-formed by the reworking of originally homogenous beds, differentiated into coarse-and-fine grained units (Belperio *et al.* 1998; Haines *et al.* 2001). The age and duration of deposition of the Kanmantoo Group is constrained by the dating of a thin felsic tuff near the top of the underlying Heatherdale Shale with a U-Pb zircon age of 526 ±4 Ma (Copper *et al.* 1992). Sandiford et al. (1992) suggest that the oldest syn-kinematic granites intruded the Kanmantoo Group at *ca* 516 Ma, while Chen and Liu, (1996) have dated post-kinematic dykes at *ca* 510 Ma and Foden *et al*, (1999) inferred syn-tectonic graintoids intruding the Kanmantoo Group has an age of 514±5 Ma.

KANGAROO ISLAND GROUP

The essentially un-metamorphosed Early to Mid-Cambrian Kangaroo Island Group is exposed at the northern end of Kangaroo Island, in the footwall of the KIFPSZ. At present-day, this group occupies an east-west trending, narrow platform (Figure 2; Flöttmann *et al.* 1995; Flöttmann *et al.* 1998). It is dominantly a clastic sequence consisting of intertidally deposited fine-grained sandstone with alluvial intercalations of coarse-grained sandstone and conglomerates (Figure 3; Daily *et al.* 1979; Daily *et al.* 1980; Macktelow 1990; Flöttmann *et al.* 1995; Flöttmann & Cockshell 1996). The deposition of the conglomerate units has been interpreted as a response to active faulting, which presumably uplifted a source area, likely to be the Yorke Peninsula (Flöttmann *et al.* 1998). The sediments of the Kangaroo Island Group represent a shallow water sequence that reflect shoreline migration as a result of syn-depositional fault uplift (Daily *et al.* 1980).

KIFPSZ on Kangaroo Island

On Kangaroo Island, the shear zone outcrops as a 1 km wide steeply dipping, obliquely transpressional displacement zone that divides two distinct geological domains; the Northern Platform Zone, and the Southern Fold-Thrust Zone (Figure 2; Flöttmann *et al.* 1995). The Northern Zone encompasses the southernmost margin of the Archaean to Mesoproterozoic Gawler Craton, which is overlain by up to 2000 m of Kangaroo Island Group sedimentary rocks (Belperio & Flint 1992). The Northern Platform Zone decrease in deformation intensity away from the KIFPSZ (James & Clark 2002). The Southern Fold-Thrust Zone, which is dominantly Kanmantoo Group rocks, appears to be dominated by a single generation of tens-of-metres to kilometre-scale east-northeast to west-southwest trending folds that are separated by fault-related folding (Flöttmann *et al.* 1995). The Spring Inlet Shear Zone, which was considered by Flöttmann *et al*, (1995), to be a south-eastern branch of the KIFPSZ, is now considered an independent parallel structure of the Southern Platform Zone (James & Clark 2002). Outcrop of the KIFPSZ is variable across the island with approximately 2 km of exposure in the Kangaroo Gully and Snugg Cove areas (Figure 2). It then bends seawards and reappears onshore to the east of Western River Cove. There is little to no exposure in the centre of the island towards the east until Point Morrison/American River (Flöttmann *et al.* 1995). The shear zone is defined as undifferentiated, mylonitised Kanmantoo Group sediments that are re-crystallised, fine-to-medium-grained, grey quartz phyllonite and phyllite. However, the degree of deformation appears to vary along strike of the shear zone, with highly deformed rocks observed on the

western end of the island and more widely distributed high strain zones with less intensely developed mylonites at the eastern end of the island (Flöttmann *et al.* 1995).

KIFPSZ on the Fleurieu Peninsula

Along the Fleurieu Peninsula the KIFPSZ and other parallel structures are expressed as series of northeast-southwest-treading thrust faults with dips varying between 15-35° towards the south-east (Jenkins & Sandiford 1992). These thrust faults isolate a series of crystalline basement inliers and cause varying deformational styles on the footwall and hangingwall of the Adelaidean Burra Group sedimentary rocks. Cover sequences on the hanging walls of the KIFPSZ and other thrusts are sub-horizontal with little deformation but in some cases minor, upright kink-folds with weak fabrics have developed (Jenkins & Sandiford 1992). Contrastingly cover sequences in the footwall show localised intense deformation (Macktelow 1990; Jenkins & Sandiford 1992). On the mainland, the KIFPSZ clips the north-western toe of the Fleurieu Peninsula and runs through Little Gorge (Figure 1b), where basal conglomerates of the Burra Group are highly stretched and have strong lineated fabrics. Strain on the mainland appears to be more pervasive than at Point Morrison but similar in style to deformation at Snugg Cove.

ANALYTICAL METHODS

Field Work

Field work was conducted in three phases with a total of two weeks of work completed on Kangaroo Island in early May and June 2011. Field work on the mainland was undertaken as a series of day trips in August and September. The locations were chosen based on previous mapping, location within the shear zone complex and accessibility (Fairclough 2008). Detailed transects were made perpendicular to the strike of the shear zone at Snugg Cove, Point Morrison and Little Gorge (Figure 3). Mapping and strain logs were made along these transects in order to observe the variation in strain within the shear zone. The spatial coverage, therefore, results in a rigorous dataset that allows a detailed framework to be built that characterises how the strain, orientation and transport direction has changed along the strike of the shear zone. Two transects on Kangaroo Island were chosen, for U-Pb geochronology and EBSD analysis. which will allow for a more in-depth understanding the KIFPSZ.

U-Pb of Zircons

Analytical methods for zircon separation and analysis were carried out following the method of Payne *et al*. (2008) and as outlined in Appendix 1. Three Samples from the Kanmantoo Group (Table 1; ASKI11-04, ASKI11-08, ASKI11-12) were chosen for detrital zircon Laser Ablation-Inductively Coupled Plasma Mass Spectrometry (LA-ICPMS) U-Pb analysis. U-Pb data Age

calculations were undertaken using the real time correction program GLITTER version 4.0 (Van Achterbergh *et al.* 2001).

Electron Backscatter Diffraction Analysis

Electron backscatter diffraction methods can be used to obtain the crystallographic orientation from a number of different mineral species (Dingley 1984; Lloyd 1987; Schmidt & Olesen 1989; Dingley & Randle 1992; Prior *et al.* 1999). To obtain optimum EBSD signals, indexing resolutions are highly specimen, sample-preparation and instrument dependant (Prior *et al.* 1999). Samples were prepared using previously suggested methods and according to the dimensions of the specimen chamber used (Lloyd 1987; Prior *et al.* 1999).

EBSP analysis on a Phillips XL30 Scanning Electron Microscope (SEM) was undertaken to obtain crystallographic orientation data for 5 samples from within the KIFPSZ (Table 1). Quartz-rich samples were the focus of EBSD analysis, from which crystallographic preferred orientations (CPOs) were acquired to further understand strain partitioning. Quartz was the chosen mineral for analysis for two reasons; (1) Quartz is well established in the use of EBSD techniques, and other microstructural analysis (Lloyd & Ferguson 1986; Lloyd & Freeman 1991; Pauli *et al.* 1996; Prior *et al.* 1999; Toy *et al.* 2008) and; (2) The KIFPSZ predominantly deforms sandstones and sedimentary packages. Therefore quartz rich samples can be readily found, allowing for the sampling of the same medium, which will allow for more sound comparisons across the shear zone. CHANNEL 5 software was used to index the EBSPs, the HKL

CHANNEL 5 software package “Mambo” pole plotting application. For detailed methodology and sample preparation see Appendix 1.

Seismic Interpretation Methods

Four seismic lines previously obtained by PIRSA, have been interpreted using Kingdom SMT and by hand on lines, 92DME-1, 94DME-12, 92-13 and MESA96-1 (Figures 4-8).

For the scope of this project seismic lines were used to identify faults and potential shear zones and their approximate orientations. There is no velocity profile to undertake a depth conversion, thus, lines have not been converted to depth. This is important when considering the dip of faults and geometry of folds as these can change with depth conversion. Faults and shear structures were picked out by looking for reflector terminations; fault related folding was picked by reflector curvature and in some cases by changes in seafloor bathymetry.

RESULTS

Field Work

OBSERVATIONS FROM POINT MORRISON

Point Morrison is a large headland that lies 50 km from Penneshaw and 60 km from Kingscote on the eastern side of Kangaroo Island, and is approximately 8 km from American River (Figure 2). This section offers 2.5 km of coastal outcrops with steep cliffs limiting access to outcrops

along the southern part of the headland. This area is defined by a number of smaller, more discrete shear zones rather than being pervasively deformed. It has not been divided into individual domains as this area shows more gradational strain change (Figure 10). Moving south from the northern tip of Point Morrison, a pervasive southeast dipping shear fabric dominates psammitic rocks. This shear fabric forms lithons and fault-bound horses that are separated by millimetre-laminated sheared mylonites. These shear fabrics appear to truncate a number of disharmonic sheath folds and rootless folds. These folds have axial planes dipping to the southsouth east. Moving south along the section the bedding becomes more apparent and dipping to the south east, with many z-verging asymmetric folds (Figure 12a). These folds imply an antiform to the south. Discrete millimetre-laminated shear zones that are a metre wide also occur. Distinct bedding becomes evident 500 m south from the tip of the headland. Still psammitic, bedding is relatively shallow with large open and upright folds that generally plunge to the south east. The beds gradually change dip direction to the south and cross-bedding becomes more apparent. Cross-bedding relationships indicate that the sequence is overturned and younging direction is to the north (Figure 12b). The bedding appears to indicate a map-scale antiformal syncline south of the highly sheared northern most point of the headland. From measuring outcrop scale folds (Figure 12a and Figure 12c), this map-scale structure has an axial plane steeply dipping to the northeast and plunging in the same general direction. A steeply south dipping foliation becomes more intense to the southern edge of this area. This fabric starts to overprint the bedding with upright southeast dipping symmetrical folds becoming increasingly dominant. North of Norma Cove, the cleavage becomes more pervasive and is gradually replaced by a strong shear foliation within very intensely folded phyllonites that have excellent southeast plunging mineral lineations. South of Norma Cove, bedding reappears with tight asymmetric

folds and discrete metre- wide millimetre- laminated shear zones. These shear zones appear to be cutting the south dipping sandstone beds. Further along, the bedding becomes shallower with more overturned cross beds and open folds in what could be another map-scale antiformal syncline. The section along Point Morrison appears to show a repetition of shear zones, 50-100 m wide, which dissipate into less sheared zones with more bedding, that turn into 20-50 m wide antiformal synclines, which are juxtaposed to wider shear zones (Figure 11). The Point Morrison is as an area that has more widely distributed high strain zones with less intensely developed mylonites and more discrete thrusts and large-scale complex folds than those found at Snugg Cove.

OBSERVATIONS FROM SNUGG COVE

Located on the north-west coast of Kangaroo Island 40 km west of Parndana (Figure 2), rocks at Snugg Cove belonging to the Kanmantoo Group have been sheared into a 1 km wide shear zone. Quartz veining is common within the fine, micaceous interbedded sandstones. Cliffs and current day sea-level have restricted field work in certain areas. This section is divided into three distinct domains which have been separated based on the degree and style of deformation.

Domain 1

This domain runs along the northern side of the cove and up into scree covered steep cliffs, which consists of interbedded psammites and pelites that are extremely well cleaved. These planar cleavage surfaces have prominent ribbing down dip that appears to be bedding traces on

the cleavage planes. Bedding is centimetre to decimetre spaced (Figure 15f) with the cleavage-bedding intersections forming the prominent lineation. Rodding on quartz veins is also present. Cleavage is dipping to the southeast and bedding dips steeply to the southsouwest. Average intersection lineations plunge 44→155. There are also small-scale folds and outcropping rocks are cut by small-scale thrusts. See Figures 13-15 for maps, strain logs and outcrop images.

Domain 2

This domain dominates the central section of the cove and continues south for about 75 m. The southern side of the cove has very extensive cliffs and outcrops are limited due to present-day sea level (Figure 14b). The area is comprised of psammitic quartz and muscovite rich, well-foliated phyllonites interlayered with less than five centimetre thick quartz-rich sandstone layers (Figure 14f). Foliations are millimetre spaced and mineral elongation lineations run down dip to the southeast. Foliation and bedding are parallel and appear to be relatively planar and coherent, dipping shallowly to the south. Shearing and deformation manifest in folds and decimetre-scale faults with folded decimetre layered sandstones that are cut by low angle thrusts (Figure 15c -d). Fold hinges and axial planes shallowly plunge to the southwest and quartz boudins show excellent σ-structures indicating top to the north transport (Figure 15a). Stretching mineral lineations also indicate transport with northwest-southeast directions. Shear surfaces are rich in muscovite with well-developed C`-fabrics dipping shallowly to the southwest. Towards the southern edge of this domain, metre thick biotite-rich pelitic layers become increasingly dominant with boudinaged quartz veins (Figure 15f), some of which are deformed with δ-type fabrics giving excellent top to the northwest kinematics. The axis of rotation of these quartz

boudins plunges to the southsouwest. See Figures 13-15 for maps, strain logs and outcrop images.

Domain 3

Along the south side of the cove the rocks change from the more psammite rocks in Domain 2 highly sheared pelitic rock with millimetre- to centimetre- biotite and muscovite layers that are extensively foliated (Figure 15f). The average foliation in this domain is 45° to the south, which shows no change from the previous domain. The high abundance of quartz vein boundins (Figure 15f), which are associated with biotite-chlorite and muscovite, are strongly rodded. The axis of rotation of these quartz boudins is 45° to the northeast. There are a number of centimetre- to decimetre- scale folds that along with asymmetric near isoclinal folds, verging to the north. Stretching mineral lineations plunge 43° to the southeast, which suggests that transport direction was orientated northwest-southeast. Boudinaged quartz veins are deformed with some δ-type fabrics giving excellent top to the northwest kinematics. Fold hinges are also parallel to the mineral lineation. A 1 m thick layer of massive conglomerate/gritty sandstone occurs that is preferentially weathered to produce a small elongate cave in the middle of this domain. Descriptions of fold styles, veins and tectonic structures indicate that the shear zone formed by progressive simple shear in high strain zones, with a transport direction of top to the north and north-west.

OBSERVATIONS FROM LITTLE GORGE

The section at Little Gorge encompasses Mesoproterozoic to Paleoproterozoic basement and Burra Group sedimentary rocks. These sediments have been folded, overturned and thrust with mineral lineations and quartz fibres that plunge towards the southeast and kinematic indicators that show top to the north-west-directed displacement. Little Gorge lies along the western coast line of the Fleurieu Peninsula about 10 km south of Normanville (Figure 16b). The section runs from the western coastal margin, east into the gorge and surrounding hills. Starting from the waterline and moving progressively inland, the coastal outcrop can be divided into two areas; dominantly conglomerates and coarse-grained sandstones (Figure 16 and Figure 17f) to the west and fine-grained pelitic and boudinaged pegmatites along the eastern coastal section. Along the entire section, the rocks consistently dip to the east. These two broad areas can be further divided with the most western section being a highly sheared and foliated quartz arenite that has metre-scale cross-cutting shear surfaces and cross-bedding (Figure 17a). This section appears to be highly sheared with 10% heavy mineral layers and well-developed streaky lineations on the surface, which plunge to the south east. Moving east, this area abruptly turns into a 2 m thick limestone layer that is severely weathered. To the east of this the cross-bedded quartz arenite becomes dominate again, with excellent extensional streaky lineations on the bedding surfaces. These cross-beds look inverted with truncation surfaces at the base of decimetre thick foresets. A 10 m thick unit of conglomerates and coarse-grained lithic arenite sits adjacent to the cross-bedded unit (Figure 17e). Clasts are <50 cm and are very highly stretched, indicating a high degree of strain. The rocks closest to the beach change into highly strained pelites/phyllites. These have very elongate stretching lineation fabrics and good top to the north-west σ-kinematics. The hilly inland outcrops are separated by 50 m of sand and scree. Up the hill at the

base of the cliffs excellent examples of C-S fabrics are exposed in sheared coarse-grained sandstone/granule conglomerate (Figure 17b). Moving northward along the cliff top, pale metre-scale boudins of granite that are inter-sheared within a mylonite fabric showing C-prime fabrics (Figure 17c). These rocks appear to represent the same pelitic unit observed on the beach, but metamorphosed to slightly higher grade. Moving east and into the gorge, the groundmass in rocks here has much more potassium feldspar than other sheared units in the section, which could indicate lower strained basement. This basement appears to be highly sheared with pods, lenses and clasts of potassium feldspar; potassium feldspar and quartz and pure quartz. Two-hundered metres into the gorge, outcrops of migmatitic orthogneiss are cut by a 30-40 m wide potassium feldspar and quartz leucosome (Figure 17d).

U-Pb Zircon Geochronology

Zircon geochronology results are presented as probability density diagrams (Figures 18a-20a), concordancy diagrams (Figure 18b-20b), and all relevant data are presented in Table 1. $^{206}Pb/^{238}U$ ages are used for zircons that are <1000 Ma, where as $^{207}Pb/^{206}Pb$ ages are used for zircons >1000 Ma. Cathodoluminescence (CL) images (Figures 18c-20c) were used to determine which grains were targeted; grains displaying oscillatory zoning were targeted to give the highest likelihood of dating magmatic crystallisation ages of source rocks. Well-exposed rims were targeted on some samples, as well as zircon grains with no distinguishable magmatic cores, to determine the timing of metamorphism of source rocks. In all three samples core and rims offered no variance in ages. For description of sample location, and lithologies see Table 1. For details on zircon grain size, shape, colour and CL descriptions see Table 2 and Figures 18c-20c.

ASKI1108

The zircons from within this sample show a great deal of heterogeneity (Table 2). One- hundred- and- forty- six analyses where undertaken from 120 individual zircon grains. Forty-four of the 142 spots were between 90-110% cordandant. The U-Pb analyses yielded a large spread of data with two distinct peaks at *ca* 1200-1100 Ma and 650-570 Ma and smaller peaks at *ca* 2500 Ma and 2240 Ma (Figure 18a). The youngest population of detrital zircon grains give a weighted average of 587 ±17 Ma and is considered to be the maximum depositional age. The youngest concordant analysis yielded a $^{206}Pb/^{238}U$ age of 556 ±19Ma (Figure 18c).

ASKI1112

One- hundred- and- thirty- two spots were analysed on 100 grains with 61 of these spots being between 90-110% concordant. Two main zircon populations occur at *ca* 650-600 and 1100-1000 Ma with three smaller peaks at *ca* 2300 Ma, 2700 Ma, and 3000 Ma. The youngest concordant grain gives a $^{206}Pb/^{238}U$ age of 546 ±7 Ma (Spot 35; Figure 19c). The youngest population of detrital zircon grains give a weighted average of 617 ±5 and is considered to be the maximum depositional age.

ASKI1104

Zircons in this sample are heterogeneous and vary in size, shape, texture and origin (Table 2) Thirty three of the 89 spots were found to be 90-110% concordant. The U/Pb analysis yielded a large spread of data with two distinct peaks at *ca* 600-560 Ma and 1100-1000 Ma and a number of older minor peaks ranging from *ca* 2240 Ma and 2500 Ma (Figure 20a). Of the concordant data the youngest spot analysed was spot 143 (Figure 20c) that yielded a $^{206}Pb/^{238}U$ age of 547 ±7 Ma (93% concordancy). The youngest population of detrital zircon grains give a weighted average of 623 ±31 Ma and is considered to be the maximum depositional age.

Electron Backscatter Diffraction

A number of automated beam maps were made from five samples from within the KIFPSZ (ASKI11-03, ASKI11-04, ASKI11-05, ASKI11-06 and ASKI1112). For sample locations and lithologies see Table 1. The maps were run with 1µm step sizes on areas that were dominated by quartz. Indexing rates varied between samples and locations, the averages of which can be seen in Table 3.

Automated map files were combined into single projects for each sample and stereographic data plots of quartz <c> axis (0001) and <a> (11-20) axes were created using the HKL CHANNEL 5 software package 'Mambo' pole plotting application (Figures 22). Stereographs are presented with the Y-direction of finite strain vertical and the X- and Z-directions along the east-west and north-south axes. This allows for corresponding foliation and lineation to be presented as an eas-west trending vertical plane and horizontal line. Both pole plots and contours were composed using 24° half width and 5° data clustering. Crystallographic preferred orientation (CPO)

stereographs show which grains in an aggregate have a particular orientation giving patterns that can appear as point maxima or as small or great circle girdles.

Table 3 provides foliation and lineation data and a summary of the EBSD pattern descriptions and their potential slip mechanisms. Slip mechanics have been inferred using (Figure 23a-c) from (Schmid & Casey 1986; Passchier & Trouw 2005).

Seismic Interpretation Results

Faults and associated fold structures were interpreted from four seismic lines (Figure 4). A total of 20 faults were interpreted, which all strike northeast-southwest and dip moderately to the southeast (Figures 5-8). These faults not only offset the older, Cambrian strata but also offset and in some cases cause fault-related antiforms in the younger sediments, frequently expressed in the sea-floor bathymetry. These faults appear to have reverse displacements. The lines also show that the structures that are observed on the mainland can be extrapolated offshore and connect with structures on Kangaroo Island. Table 4 shows a full list of structures and orientations that were interpreted from the four seismic lines.

LINE 92-13

This line is orientated southeast-northwest and four faults have been interpreted on this line (Figure 6). These faults dip to the southeast. Three of the lines are associated with antiforms that

appear to be verging to the west. The faults form a series of imbricates with a detachment depth varying from 1.5 seconds (~1 km) to about 1 second (0.850 km).

LINE 92DME-1

Of the nine faults that have been interpreted on this section (Figure 7), seven of them form a duplex style structure with a detachment occurring at 3.5 seconds (~2.5 km). This structure is plunging to the southeast. There are two other reverse faults that are dipping to the southeast. There is a significant amount of shortening accommodated along these structures.

LINE 94SME-12

Only three faults have been interpreted on this section (Figure 5), which form broadly 100 m spaced imbricated faults. Three antiforms have formed as a result of these faults and they appear to be displaying a significant degree of shortening. The antiforms are verging to the northnorthwest and have developed in the hanging wall.

LINE MESA96-1

Two of the five faults observed have caused the formation of antiforms, the other three appear to offset the upper sediments and run through to the sea floor (Figure 8). This, coupled with fault susceptibility diagrams suggests that these faults are active at the present day. These south-

dipping structures represent multiple imbricate faults that have accommodated a significant amount of shortening.

DISSCUSSION

Provenance of the Kanmantoo Group

Understanding the provenance of the deformed Kanmantoo Group is extremely important in providing a reconstruction of the tectonic setting and structural framework during deposition and subsequent deformation, and further, it provides information that can assist in modelling ancient continental reconstruction. There are a number of possible sources for the Kanmantoo Group sedimentary rocks, which have been highlighted by previous studies (Turner *et al.* 1993; Ireland *et al.* 1998; Haines *et al.* 2004; Haines *et al.* 2009).

The Kanmantoo Group has been constrained as having a window of only approximately 12 million years for deposition of the estimated 7-8 km of sediments (Copper *et al.* 1992; Sandiford *et al.* 1992; Chen & Liu 1996; Foden *et al.* 1999). This equates to a sedimentation rate of approximately 150 cm/y. Such high rates of sedimentation strongly suggest some tectonic influence on accommodation space, as well as a tectonically active source area, for example a hinterland to foreland basin. However, the fine and unimodal grain distribution of the sandstone infers that the Kanmantoo Trough was somewhat distal from the source area (Haines *et al.* 2001).

Detrital zircon data provides the best initial criteria for identifying suitable terrains as sediment sources. Age spectra for the three samples, when plotted together (Figure 21b), show similar patterns with two main populations at 700-500 Ma and 1300-900 Ma and a number of scattered older peaks from 3500 to 1500 Ma. These U-Pb age peaks from the Kanmantoo Group, suggest that they are likely to be derived from a source region containing abundant Neoproterozoic to Cambrian zircons, coupled with a large amount of late Mesoproterozoic ages and minor Mesoproterozoic and Archean terrains. Based on current Gondwana reconstruction models (Li *et al.* 2008) and information on the spatial relationship of the Kanmantoo Trough (Belperio & Flint 1992; Flöttmann *et al.* 1998) to surrounding terrains during deposition, the source to the Kanmantoo Group sediments can be likely confined to Australia and Antarctica (Figure 24).

Though Adelaidean Basin sediments, such as the Marino Arkose, the Bonney Sandstone and the Heatherdale Shale, show significant peaks between *ca* 1200-900 Ma, and have a number of scattered older peaks from *ca* 3500 to 2000 Ma, they lack substantial *ca* 700-500 Ma zircon populations (Ireland *et al.* 1998). These Adelaidean sequences also have a large amount of 1650-1450 Ma detritus, which is missing from the Kanmantoo Group sediments (Ireland *et al.* 1998). Sm-Nd isotopic evidence by Turner *et al.* (1993) show that the Kanmantoo Group have significantly lower ε_{Nd} values than that of the Adelaidean Basin. It is therefore unlikely that the source of the Kanmantoo Group is simply sourced from the Adelaidean sequence. Furthermore, the model ages of the Adelaidean Basin are significantly older, which rules out simple reworking on the Adelaidean sediments (Turner *et al.* 1993). These results suggest that the Kanmantoo

Group sedimentary rocks could be derived from a mixture of basement and reworked Adelaidean or the mixing between older Gawler Craton basement material and reworked Neoproterozoic material (Turner *et al.* 1993). ε_{Nd} values from the Kanmantoo Group sedimentary rocks contradict simple mixing/unmixing, and infer a more complex, multi-source provenance (Haines *et al.* 2009). Detrital muscovite ^{40}Ar-^{39}Ar studies also suggest that the provenance of these sediments differ from that of adjacent basins at the time of deposition (Haines *et al.* 2004).

Identifying a more complex, multi-source provenance for the Kanmantoo Group sediments, as proposed by Haines et al. (2009), is a non-trivial exercise. Sources must satisfy the spectrum of U-Pb zircon data collected; i.e. detrital zircons must span age brackets of both *ca* 700-500 Ma and 1200-900 Ma. The Musgravian Orogeny and the Albany–Fraser Orogeny (Figure 24) both caused extensive reworking of Australia during the late Mesoproterozoic, and therefore, are potential sources for Mesoproterozoic detritus (Kirkland *et al.* 2011; Smithies *et al.* 2011). The Ross and Petermann Orogenies (Figure 24) also involved extensive reworking during the Ediacaran-Cambrian, and therefore, could feasibly be the source for the younger *ca* 650-500 Ma detrital zircon ages observed. The Musgravian and the Albany–Fraser Orogens are broadly synchronous, and therefore, yield U–Pb zircon ages in the range of 1200–1100 Ma (Kirkland *et al.* 2011; Smithies *et al.* 2011) the Musgrave Province was then reactivated during the latest Neoproterzoic to early Cambrian Petermann Orogeny (Hand & Sandiford 1999; Raimondo *et al.* 2009, 2010). Metamorphic zircon growth or recrystallisation during the Petermann Orogeny is constrained between 575 Ma and 535 Ma (Hand & Sandiford 1999; Raimondo *et al.* 2009, 2010). However, the Petermann Orogeny can be ruled out as it developed in an intracratonic setting with very little associated igneous activity (Hand & Sandiford 1999; Raimondo *et al.*

2009, 2010) and the *ca* 700-500 Ma zircon grains found in the Kanmantoo Group samples include considerably igneous zircon grains. The Musgravian and Petermann orogenies have been thought to be a significant source of the Marino Arkose Member, of the Wilmington Formation, within the Adelaidean Basin (Preiss 2000). Previous ^{40}Ar-^{39}Ar geochemistry and further isotopic studies discussed earlier, suggest that the Kanmantoo Group sediments are derived largely from rocks not available at the time the Adelaidean Basin was being deposited (Turner *et al.* 1993; Haines *et al.* 2004; Haines *et al.* 2009). This evidence implies that the Musgravian and Petermann orogenies cannot provide a provenance for both sedimentary successions. Before re-evaluating the provenance of certain Adelaidean Basin sediments, a better fit for provenance for the Kanmantoo Group may be found elsewhere.

Some authors have suggested the Ross Orogeny (Figure 24) to be the most likely source of the Kanmantoo Group, or at least the younger population of zircons (Flöttmann *et al.* 1998; Ireland *et al.* 1998). This concept appears to satisfy many current models for plate reconstructions during the late Neoproterozoic-Early Cambrian. However, this model is not supported by other geological evidence. The Ross Orogeny lacks known magmatism older than 550 Ma, and therefore, does not account for a significant proportion of the data (Boger 2011). Haines et al. (2004) also highlights that many of the detrital ^{40}Ar-^{39}Ar results mirror those of U-Pb zircon age spectra. There is a high yield of detrital muscovite from within the Kanmantoo Group, and muscovite is considered to be rare in convergent margin volcanic rocks. Thus the Ross Orogeny is not considered a source of provenance (Haines *et al.* 2004). Additionally, there is growing recognition of the increasingly widespread nature of the 650–500 Ma zircon age signatures,

which have now been found within the Pan-Gondwana orogens in Western Australia and Antarctica (Boger 2011).

These Pan-Gondwanan orogens are now considered to be spread across Western Australian, with the Leeuwin Complex of the Pinjarra Orogen, east Antarctica and India, linking the Prydz–Leeuwin Belt, to the Mozambique Orogenic Belt (Figure 24; Veevers 2006; Veevers 2007). Importantly, terrains from within these orogens provide similar age signatures to those found in the Kanmantoo Group. Veevers (2006) speculated that this orogenic belt may extend in a broad zone beneath the east Antarctic ice sheet, into central Antarctica, where it manifests as the Gamburstev Subglacial Mountains. Detrital zircon patterns from Antarctica present a correlation that can be seen between certain areas and the Kanmantoo Group (Figure 21). The four prospective regions from within Antarctica are Prydz Bay, Central Antarctica and the Prince Charles Mountains.

The compilation of zircon data from Prydz Bay encompasses data from units making up the Prydz–Belt (Veevers *et al.* 2008a). Rocks have come from glacial erratics that are interpreted to originate from central Antarctica or the Gamburstev Subglacial Mountains, which are thought to have been an extension of the Prydz-Leeuwin Belt under the east Antarctica ice sheet (Veevers *et al.* 2008a). The two major peaks expressed in the Prydz Bay zircon data set are similar to those of the Kanmantoo Group (Figure 21). The early peak correlates well, however, the late Mesoproterozoic peak lacks significant *ca* 1300-1200 Ma zircons (Veevers & Saeed 2008b; Veevers *et al.* 2008a). The older intermittent peaks also correlate well and there is a significant

gap in zircons at 1300-1400 Ma, which is noteworthy in the Kanmantoo Group data (Figure 21). Haines et al. (2009) also speculated that the Prydz-Belt could be a suitable source for provenance given its Neoproterozoic to early Paleozoic magmatism and its similar Sm-Nd signature to that of the Kanmantoo Group. The U-Pb zircon dataset appears to support the concept that the Prydz-Belt as a source for the Kanmantoo Group.

Data from central Antarctica shows correlation with that of the Kanmantoo Group, with both the Late Neoproterozoic- Cambrian and Mesoproterozoic peaks matching well (Figure 21; Veevers & Saeed 2007; Elliot & Fanning 2008; Goodge *et al.* 2008). However, there is a lack of 1900 Ma or older detritus and the 1550-1450 Ma peak is not reflected in the Kanmantoo Group at all.

The distribution of ages found in the Prince Charles Mountains has a very similar patter to those found in the Kanmantoo Group (Veevers & Saeed 2008a; Veevers *et al.* 2008b). The 650-500 Ma peak, though slightly smaller, is present with the 1300-900 Ma peak. The lack of 1900-1400 Ma ages is also seen in rocks from this area, yet the older, pre-1900 Ma ages appear to be very dominant. Though this area has a 650-500 Ma peak, these results were obtained from detrital zircons from sandstones that would have been depositing around the same time as the Kanmantoo Group, and would need to have been sourced from elsewhere (Veevers & Saeed 2008a).

When there are a number of terrains competing as potential sources, paleoflow directions can be useful. Assessment of paleocurrent directions conclude that the bulk of sediment transport direction in most of the Kanmantoo Group was essentially from the south (Figure 24; Haines *et al.* 1996; Flöttmann *et al.* 1998; Haines *et al.* 2001). Considering the spatial relationships of the potential terrains to the Kanmantoo Trough; the Prince Charles Mountains may be too far to the west to provide sedimentation derived from the south. Rocks of the Prydz Bay area, and subsequent Prydz-Belt coupled with rocks from Central Antarctica and Gamburstev Subglacial Mountains appear be the best localities based on paleocurrent indications.

Squire et al. (2006) has speculated that the appearance of quartz-rich sedimentary units with prominent 650-550 Ma and 1200-900 Ma zircon age peaks deposited during the Early Cambrian are likely a result of large-scale sedimentary fans from an extensive 'Transgondwana Supermountain'. There is evidence to suggest this may be true, in particular the abundant turbidites deposited throughout the Kanmantoo Group and their ages are similar to other similar systems around the globe. However, there are a number of other sources that could provide sediments into the Kanmantoo Basin that are more proximal. The Kanmantoo Group was sourced from a mixture of different terrains, thus, the most likely source of provenance may not be confined to the one location that simply provides the best U-Pb correlation. The Kanmantoo Group was deposited as a result of rapid tectonic uplift, as a foreland basin, depositing a series of sediments thought to represent a shallow water, slope and rift environment (Daily & Milnes 1973; Daily *et al.* 1979; Gatehouse *et al.* 1990; Gravestock & Gatehouse 1995; Belperio *et al.* 1998; Jago *et al.* 2003). Thus it is highly probable that relative uplift in Antarctica resulted in sediments being sourced from then exposed rocks in central and southern and Antarctica.

Geographically, and based on U-Pb zircon geochronology and other provenance techniques found in the literature, the most probable source terrains are to be found in the Prydz section of the Prydz-Leeuwin Belt and the Gamburstev Subglacial Mountains (Figure 21 and Figure 24).

The Strain Evolution of the KIFPSZ

Deformation associated with shear zones may be both spatially and temporally variable resulting in a complex interplay of structures developed across a range of scales (Alsop *et al.* 2004). It is therefore necessary to consider the relationships and interactions of the crustal, regional, outcrop and microscopic controls in order to gain a complete understanding of shear zone processes and their strain evolutions (Alsop *et al.* 2004). In crustal-scale shear zones, like the KIFPSZ, the accommodation and distribution of strain may vary spatially and also temporally and pure and simple shear deformation may be simultaneous partitioned within the shear zone (Tikoff and Teyssier 1994; Jones and Tanner 1995; Dewey et al 1998; Lin and Williams 1998; Reddy et al 1999, 2003). In determining the strain evolution of the KIFPSZ microscopic–scale and macroscopic-scale deformation for each location needs to be discussed, compared and put into a crustal-scale context.

MICROSCOPIC-SCALE STRAIN PARTITIONING

Whilst it can be observed at outcrop scale how strain partitioning varies along the KIFPSZ and can be used to extrapolate more crustal scale consequences, the microscopic observations and variances offer more subtle differences. The quartz CPO patterns measured along the KIFPSZ

appear to represent a variety of active slip-systems during deformation (Figure 23). The relationship between the locations of the c-axis peaks on stereographic projections (Figure 22) can be associated with different slip-planes (Figure 23a; Schmidt & Olesen 1989; Passchier & Trouw 2005; Toy *et al.* 2008). The type of slip-system that will be active in a crystal depends on the orientation and magnitude of the stress field and the critical resolved shear stress (CRSS) for a particular slip-system (Passchier & Trouw 2005). The CRSS is strongly dependant on temperature, strain rate and differential stress, as a result of which, the types of slip-systems active change with metamorphic and stress conditions (Passchier & Trouw 2005).

Interpretations of quartz CPO strain fabrics were made by comparing them against diagrams in (Schmid & Casey 1986; Schmidt & Olesen 1989; Passchier & Trouw 2005; Toy *et al.* 2008; Figure 23). In non-coaxial deformation basal <a>, rhomb <a> and prism <a> slip systems operate along the <a> axes. With increasing temperatures and/or stress regimes, basal<a> and then rhomb<a> cease respectively, and prism <a> slip dominates. Post ~ 650 °C <a> axis deformation stops and is replaced by <c> slip movement.

Samples ASKI11-05 ASKI11-06 ASKI11-12 are all from within the Snugg Cove section on the western end of the shear zone (Figure 14). The samples are taken from areas of increasing strain starting with ASKI11-12 then ASKI11-05 and ASKI11-06 (Figure 14), with the CPO patter reflect a change in strain intensity. ASKI11-05 expresses a cleft girdle with two small circles around the z-axis. The symmetrical nature of this pattern indicates co-axial deformation implying flattening strain dominates this sample (Passchier & Trouw 2005; Toy *et al.* 2008). This

correlates with field observations as the sample was taken from a quartz-rich layer near boudinaged quartz veins. ASKI11-06 which exhibits non-coaxial asymmetry has c-axis maxima indicating a combination of prism <c> and basal <a> slip mechanics (Figure 22 and Figure 23c). ASKI11-12 shows two point maxima indicating basal <a> and rhomb <a> slip-systems (Figure 22 and Figure 23c). The CPO's express a gradual increase in temperature or stress as different slip systems operate. As these samples are spatially close, it seems unlikely that they would have experienced much temperature difference during deformations, and outcropping rocks do not indicate dramatic temperature increases over a 200 m transect. This coupled with outcrop observations suggests that there is a progression from lower strain intensity with basal<a> and rhomb <a> to higher strain intensity with coaxial patterns, to basal <a> and high stain prism <c> slip mechanisms. The gradual increase is strain is also reflected in outcrop scale (Figure 14).

CPO's from samples from Point Morrison are taken from two ends of the largest shear zone (Figure 11). The two samples though, spatially close, present different CPO's. ASKI11-03 exhibits a CPO that is asymmetrical and non-coaxial and appears as a single girdle fabric resulting from a combination of prism <a>, rhomb <a> and basal <a> slip systems (Figure 22 and Figure 23c). ASKI11-04 is also asymmetrical and non-coaxial, but does not form a girdle. Instead, it has a dominant c-axis maxima/peak that suggests rhomb <a> slip and what could be a faint prism <c> slip maxima (Figure 22 and Figure 23c). The combination of prism <a> rhomb <a> and basal <a> active slip-systems expressed in ASKI11-03 suggests a temperature range of 450-550°C during the alignment of quartz grains (Schmidt & Olesen 1989; Dingley & Randle 1992; Pauli *et al.* 1996; Leiss *et al.* 2000; Passchier & Trouw 2005; Toy *et al.* 2008). In comparing this with the observed metamorphic grade of rocks at Point Morrison, which do not

appear to have reached such high temperature, the active slip-systems would most likely have been cause as a result of increasing strain conditions. Deflections at the ends of single-girdle fabrics expressed in ASKI11-03 reflect an anti-clockwise rotation that could indicate a sinistral shear sense of shear (Passchier & Trouw 2005). Once considered in context to the external reference frame, this shear sense indicates top-to-the-north displacement. Toy et al. (2008) have also shown that in the Alpine Fault that such patterns can be used as kinematic indicators. Using such patterns for shear sense does however need to be coupled other valid data, which in this case corresponds with field observations and documented displacement along the KIFPSZ (Flöttmann *et al.* 1995).

The marked asymmetry of CPO's described indicates a domination of simple shear deformation within the shear zone. However, there is a domain that exhibits more symmetrical quartz fabrics, ASKI11-05, that represents more co-axial, pure flattening strain. The strong and consistent asymmetry displayed by nearly all the CPO's indicates a high ratio of simple to pure shear with shear sense of top to the north-west.

MACROSCOPIC-SCALE STRAIN PARTITIONING

Outcrop scale mapping and strain logs highlight varying degrees of strain partitioning and orientation (Figure 11, Figure 14 and Figure 16). Litholological controls like composition, mineralogy and grain size have had an effect on the shear zone development. This is evident in way the KIFPSZ is manifested in the Kanmantoo Group sediments verse the Burra Group

sediments of the Adelaidean Basin. Deformation within the same sedimentary groups also show varying degrees of heterogeneity. This may have more to do with local environmental conditions of pressure, temperature and strain rate effects on shear zone processes. In all three of the locations within the KIFPSZ, the way in which strain is manifested appears to differ (Figure 11, Figure 14 and Figure 16). Whilst mineral lineations remain relatively consistent, foliations and bedding gradually rotate into a more easterly direction at Little Gorge (Figure 11, Figure 14, Figure 16 and Figure 25).

The western end of the KIFPSZ along the Snugg Cove transect, deforms Kanmantoo Group sediments as a wide encompassing shear zone that has been divided into three domains. The deformational intensity of these domains increases southwards yet maintains similar structural orientations and shear indicators. From the northern domain (Domain 1) with identifiable bedding and a pervasive cleavage, through a gradual transition into Domain 2 where bedding becomes unidentifiable and foliation with a pronounced mineral lineation becomes the dominate structure, then into a pervasively sheared, deformed domain (Domain 3). Mineral lineations also indicate transport with northwest-southeast directions and the presence of quartz σ- and δ-inclusions indicate that the shear zone formed by progressive simple shear with top to the north transport direction.

Although the section at Point Morrison that is deforming the same lithological unit, the difference in the style of deformation is highlighted by the more widely distributed high strain zones that have less intensely developed mylonites and more discrete thrusts and large-scale

folds. In some areas along the Point Morrison section, folds and bedding have been faulted and truncated along shear planes which indicated a more brittle style of deformation. The foliation surfaces are not as rich in muscovite and there are no extensive areas of quartz veining. Mineral lineations are found to be confined to smaller-scale zones that have experiencing increased deformation. This shows that strain is manifested as a network of smaller interconnected, adjacent shears.

While comparisons between the two sections on Kangaroo Island highlight the effect that local conditions of pressure, temperature and strain rate have on the same unit, the exposed section of the KIFPSZ on the Fleurieu Peninsula deforms Burra Group. The section at Little Gorge shows deformation styles similar to those found along the Point Morrison section, coupled with the intensity of the Snugg Cove section. One of the key differences is the orientation of bedding and shear foliations, which dip in a more easterly orientation, opposed to the more southerly dips on Kangaroo Island. This change in orientation coincides with the curving nature of the SAFTB (Mancktelow 1981; Jenkins & Sandiford 1992; Belperio & Flint 1993; Flöttmann *et al.* 1994; Flöttmann *et al.* 1995; Flöttmann & Cockshell 1996; Marshak & Flöttmann 1996; Flo¨ttmann & James 1997; Yassaghi *et al.* 2000; Yassaghi *et al.* 2004; Direen *et al.* 2005; Fairclough 2008). The mineral lineations coupled with kinematic indicators suggest top to the north-west displacement.

CRUSTAL-SCALE STRAIN PARTITIONING

On a larger scale, the orientation of bedding, foliations, mineral lineations and direction of transport highlight the lithospheric-scale controls, in particular the plate boundary condition on shear zone development. This can in turn unveil important information about the formation of the SAFTB and current day activity along the fold belt. The orientation of mineral lineations remain relatively consistent along the three sections. This coupled with data collected from kinematics, which indicate top to the north and north-west, indicate a syn-orogenic curvature of the Fleurieu Arc section of the SAFTB. Studies have shown that syn-orogenic curvature results in non-rotational arcs, or primary arcs with a uniform slip (Hudleston 1973; Marshak 1988; Weil *et al.* 2010). Schematic kinematic models for such systems show that the orientation of transport does not change during the evolution of the bend (Hudleston 1973; Marshak 1988; Weil *et al.* 2010). In many cases a rigid crustal block or indentor is responsible for curvature, which in some cases can be an irregular shaped continental margin (Figure 25). The relative change in bedding and foliation is due to the angle of the ridged crustal block and where certain areas are in relation to the indentor and the propagating thrust (Hudleston 1973; Marshak 1988; Weil *et al.* 2010).

The Gawler Craton has been proposed as the crustal block responsible for curvature in the SAFTB (Figure 25; Offler & Fleming 1968; von der Borch 1980; Macktelow 1990; Belperio & Flint 1992; Jenkins & Sandiford 1992; Flöttmann *et al.* 1995; Marshak & Flöttmann 1996; Flöttmann & James 1997).The orientation of foliation and bedding within the KIFPSZ suggests that the rigid crustal block that indented this north-west propagating thrust system had an almost 90° angle. Similarities in planar structures along both the Snugg Cove and Point Morrison

sections indicate that these sections of the KIFPSZ were orientated and compressed along the same edge of the craton (Figure 25). These southerly dipping shear foliations coupled with kinematics suggest that the Kangaroo Island section of the KIFPSZ was pressed up against a southern edge of the Gawler Craton. A change in foliations on the Fleurieu Peninsula to more south-easterly dips yet similar mineral lineations shows that transport is orientated in the same direction, yet foliations are being curved around. This shows that the KIFPSZ and SAFTB are being compressed along the corner of the Gawler Craton block and that curvature was syn-orogenic.

Present day stress along the KIFPSZ and other structures comprising the Fleurieu Arc section of the SAFTB are highlighted in the interpreted seismic lines (Figures 5-8) and fault reactivation diagrams (Figure 26). The seismic reflection profiles acquired in the Gulf of St. Vincent show evidence for recent deformation that have been deformed, with reverse faults displacing Cenozoic sediments and forming antiformal structures present along the current sea floor. (Holford *et al.* 2011) have also highlight Cenozoic compressional deformation along the southern Australian Margin using similar seismic methods. Furthermore, there is geological evidence for recent over thrusting at Sellicks beach, where Cambrain sediments are overthrust Cenozoic rocks (Flöttmann & Cockshell 1996). Fault reactivation diagrams using average shear zone foliations from the KIFPSZ indicate that under any stress-regime, whether it be reverse, normal, or strike slip, the KIFPSZ would, to a certain degree, be reactivated. This data coupled with seismic and current stress orientations (Hillis & Reynolds 2000) shows that orientation present day strain along the KIFPSZ is similar to that found during the Delamerian Orogeny and the orientation of this structure is still top to the north-west

CONCLUSION

By studying the structure of the KIFPZS and the provenance of its host sediments, a number of conclusions can be made; (1) Based on rigorous U-Pb detrital zircon analysis, the provenance for the Kanmantoo Group sediments is most likely sourced from the Prydz section of the Prydz-Leeuwin Belt and the Gamburstev Subglacial Mountains, in Antarcti*ca*(2) Structure and strain partioning within the KIFPSZ through microscopic and macroscopic studies shows that strain is affected by differences in lithology and local variances in pressure, temperature and strain rate. (3) The dataset adds the knowledge of the formation of the SAFTB and orientation of the Gawler Craton by highlighting the syn-orogenic nature of curvature in the Fleurieu Arc. (4) Seismic interpretations and fault reactivation diagrams, couple with literature on present day strain indicates that present day strain along the KIFPSZ is similar to that during the Delamerian Orogeny. (5) Furthermore, the current data and interpretations suggest that models proposed by Li *et al*, (2008) and Boger, (2011) best represent ancient continental reconstructions during the Late Neoproterozoic-Early Cambrian period.

ACKNOWLEDGEMENTS

I'd like to thank Associate Prf. Alan Collins for all his help and giving me the opportunity to see some cracking geology. Thanks also go out to Dr. Rosalind King for her advice and help. Thank you to Angus Netting, Ben Wade and Ken Neubauer at Adelaide Microscope for all their help. To Alec Walsh for your support and being my fieldy and draftsman and Katie Howard for her help and knowledge on all things zircon related. Thanks to Steph for her constant supply of

baked good and the amazing group of honours students this year, thanks for making this year a blast and keeping me sane. And finally, thanks to my family and friends and The Swede for all your support and understanding.

REFERENCES

ALSOP G. I., HOLDSWORTH R. E., MCCAFFREY K. J. W. & HAND M. (Editors) 2004. *Flow Processes in Faults and Shear Zones*. Geological Society, London, Special Publications 224.

BELPERIO A. P. (Editor) 1995. *Quaternary* (Bulletin 54 edition). (The Geology of South Australia,The Phanerozoic, Vol. Volume 2). Geological Survey of South Australia Adealide.

BELPERIO A. P. & FLINT R. B. 1992. The southeastern margin of the Gawler Craton, South Australia. *Deptartment of Mines and Energy*.

BELPERIO A. P. & FLINT R. B. 1993. Geological note: The southeastern margin of the Gawler Craton. *Australian Journal of Earth Sciences: An International Geoscience Journal of the Geological Society of Australia* **40**, 423 - 426.

BELPERIO A. P., PRIESS W. V., FAIRCLOUGH M. C., GATEHOUSE C. G., GUM J., HOUGH J. & BURTT A. 1998. Tectonic and metallogenic framework of the Cambrian Stansbury Basin – Kanmantoo Trough, South Australia. . *Journal of Australian Geology & Geophysics* **17**, 183–200.

BOGER S. D. 2011. Antarctica — Before and after Gondwana. *Gondwana Research* **19**, 335-371.

BOGER S. D. & MILLER J. M. 2004. Terminal suturing of Gondwana and the onset of the Ross–Delamerian Orogeny: the cause and effect of an Early Cambrian reconfiguration of plate motions. *Earth and Planetary Science Letters* **219**, 35-48.

CHEN Y. D. & LIU S. F. 1996. Precise U-Pb zircon dating of a post-D2 meta-dolerite: constraints for rapid tectonic development of the southern Adelaide Fold Belt during the Cambrian. *Journal of the Geological Society* **153**, 83-90.

CONEY P. J., EDWARDS A., HINE R., MORRISON F. & WINDRIM D. 1990. The regional tectonics of the Tasman orogenic system, eastern Australia. *Journal of Structural Geology* **12**, 519-543.

COPPER J. A., JENKINS R. J. F., COMPSTON W. & WILLIAMS I. S. 1992. Ion-probe zircon dating of a mid-Early Cambrian tuff in South Australia. *Journal of the Geological Society* **149**, 185-192.

COSTA E. & SPERANZA F. 2003. Paleomagnetic analysis of curved thrust belts reproduced by physical models. *Journal of Geodynamics* **36**, 633-654.

DAILY B. & MILNES A. R. 1973. Stratigraphy, structure and metamorphism of the Kanmantoo Group (Cambrian) in its type section east of Tunkalilla Beach, South Australia, . *Trans., Royal Society, South Australia* **97**, 213–251.

DAILY B., MILNES A. R., TWIDALE C. R. & BOURNE J. A. 1979. Geology and Geomorphology *In:* Tyler M. J., Twidale C. R. & Ling J. K. eds., *Natural History of Kangaroo Island*, pp 1-38, Royal Society of South Australia

Adelaide.

DAILY B., MOORE P. S. & RUST B. R. 1980. Terrestrial-marine transition in the Cambrian rocks of Kangaroo Island, South Australia. *Sedimentology* **27**, 379-399.

DINGLEY D. J. 1984. Difractom From Sub-Micron Areas using Electron Backscattering in a Scanning electron Mircoscope. *Scanning Electron Microscopy* **v**, 569-575.

DINGLEY D. J. & RANDLE V. 1992. Microtexture determination by electron back-scatter diffraction. *Journal of Materials Science* **27**, 4545-4566.

DIREEN N. G., BROCK D. & HAND M. 2005. Geophysical testing of balanced cross-sections of fold-thrust belts with potential field data: an example from the Fleurieu Arc of the Delamerian Orogen, South Australia. *Journal of Structural Geology* **27**, 964-984.

DYMOKE P. & SANDIFORD M. 1992. Phase relationships in Buchan facies series pelitic assemblages: calculations with application to andalusite-staurolite parageneses in the Mount Lofty Ranges, South Australia. *Contributions to Mineralogy and Petrology* **110**, 121-132.

ELLIOT D. H. & FANNING C. M. 2008. Detrital zircons from upper Permian and lower Triassic Victoria Group sandstones, Shackleton Glacier region, Antarctica: Evidence for multiple sources along the Gondwana plate margin. *Gondwana Research* **13**, 259-274.

FAIRCLOUGH M. 2008. *Kingscote Special map sheet* (2nd edition). South Australian Geological Survey 1:250000 series.

FLEMING P. D. & WHITE A. J. R. 1984. Relationships between deformation and partial melting in the Palmer migmatites, South Australia. *Australian Journal of Earth Sciences: An International Geoscience Journal of the Geological Society of Australia* **31**, 351 - 360.

FLO¨TTMANN T. & JAMES P. 1997. Influence of basin architecture on the style of inversion and fold-thrust belt tectonics--the southern Adelaide Fold-Thrust Belt, South Australia. *Journal of Structural Geology* **19**, 1093-1110.

FLÖTTMANN T. & COCKSHELL C. D. 1996. Palaeozoic basins of southern South Australia: New insights into their structural history from regional seismic data. *Australian Journal of Earth Sciences: An International Geoscience Journal of the Geological Society of Australia* **43**, 45 - 55.

FLÖTTMANN T., GIBSON G. M. & KLEINSCHMIDT G. 1993. Structural continuity of the Ross and Delamerian orogens of Antarctica and Australia along the margin of the paleo-Pacific. *Geology* **21**, 319-322.

FLÖTTMANN T., HAINES P., JAGO J., JAMES P., BELPERIO A. & GUM J. 1998. Formation and reactivation of the Cambrian Kanmantoo Trough, SE Australia: implications for early Palaeozoic tectonics at eastern Gondwana's plate margin. *Journal of the Geological Society* **155**, 525-539.

FLÖTTMANN T. & JAMES P. 1997. Influence of basin architecture on the style of inversion and fold-thrust belt tectonics- the southern Adelaide Fold-Thrust Belt, South Australia. *Journal of Structural Geology* **19**, 1093-1110.

FLÖTTMANN T., JAMES P., MENPES R., CESARE P., TWINING M., FAIRCLOUGH M., RANDABEL J. & MARSHAL S. 1995. The structure of Kangaroo Island, South Australia: Strain and kinematic partitioning during Delamerian basin and platform reactivation. *Australian Journal of Earth Sciences: An International Geoscience Journal of the Geological Society of Australia* **42**, 35 - 49.

FLÖTTMANN T., JAMES P., ROGERS J. & JOHNSON T. 1994. Early Palaeozoic foreland thrusting and basin reactivation at the Palaeo-Pacific margin of the southeastern Australian Precambrian Craton: a reappraisal of the structural evolution of the Southern Adelaide Fold-Thrust Belt. *Tectonophysics* **234**, 95-116.

FODEN, SANDIFORD, DOUGHERTY P. & WILLIAMS 1999. Geochemistry and geochronology of the Rathjen Gneiss: implications for the early tectonic evolution of the Delamerian Orogen. *Australian Journal of Earth Sciences* **46**, 377-389.

FODEN J., ELBURG A. M., DOUGHERTY-PAGE J. & BURTT A. 2006. The Timing and Duration of the Delamerian Orogeny: Correlation with the Ross Orogen and Implications for Gondwana Assembly. *Journal of Geology* **114**, 189-210.

GATEHOUSE C. G., JAGO J. B. & COOPER B. J. (Editors) 1990. *Stratigraphy and sedimentology of the Carrickalinga Head Formation (low stand fan to high stand systems tract), Kanmantoo Group, South Australia.* (The Evolution of a Late Precambrian Early Palaeozoic Rift Complex: the Adelaide Geosyncline, Vol. Special Publication 16.). Geological Society of Australia

GOODGE J. W., MYROW P., WILLIAMS I. S. & BOWRING S. A. 2002. Age and Provenance of the Beardmore Group, Antarctica: Constraints on Rodinia Supercontinent Breakup. *Journal of Geology* **110**, 393.

GOODGE J. W., VERVOORT J. D., FANNING C. M., BRECKE D. M., FARMER G. L., WILLIAMS I. S., MYROW P. M. & DEPAOLO D. J. 2008. A Positive Test of East Antarctica–Laurentia Juxtaposition Within the Rodinia Supercontinent. *Science* **321**, 235-240.

GRAVESTOCK D. I. & GATEHOUSE C. G. (Editors) 1995. *Stansbury Basin*. (The Geology of South Australia, Volume II, the Phanerozoic, Vol. 54). Geological Survey of South Australia Bulletin

HAINES P. W., FLOTTMAN T., GUM J. C., JAGO J. B. & GATEHOUSE C. G. 1996. Integrated approach to the reinterpretation of the Cambrian Kanmantoo Group type section, South Australia. . *Geological Society of Australia Abstracts* **41**, 177.

HAINES P. W., JAGO J. B. & GUM J. C. 2001. Turbidite deposition in the Cambrian Kanmantoo Group, South Australia. *Australian Journal of Earth Sciences* **48**, 465-478.

HAINES P. W., TURNER S. P., FODEN J. D. & JAGO J. B. 2009. Isotopic and geochemical characterisation of the Cambrian Kanmantoo Group, South Australia: implications for stratigraphy and provenance. *Australian Journal of Earth Sciences* **56**, 1095-1110.

HAINES P. W., TURNER S. P., KELLEY S. P., WARTHO J.-A. & SHERLOCK S. C. 2004. 40Ar-39Ar dating of detrital muscovite in provenance investigations: a case study from the Adelaide Rift Complex, South Australia. *Earth and Planetary Science Letters* **227**, 297-311.

HAND M., REID A. & JAGODZINSKI L. 2007. Tectonic Framework and Evolution of the Gawler Craton, Southern Australia. *Economic Geology* **102**, 1377-1395.

HAND M. & SANDIFORD M. 1999. Intraplate deformation in central Australia, the link between subsidence and fault reactivation. *Tectonophysics* **305**, 121-140.

HILLIS R. R. & REYNOLDS S. D. 2000. The Australian Stress Map. *Journal of the Geological Society* **157**, 915-921.

HOLFORD S. P., HILLIS R. R., DUDDY I. R., GREEN P. F., STOKER M. S., TUITT A. K., BACKE G., TASSONE D. R. & MACDONALD J. D. 2011. Cenozoic post-breakup compressional deformation and exhumation of the southern Australian margin. . *The APPEA Journal* **51**.

HUDLESTON P. J. 1973. Fold morphology and some geometrical implications of theories of fold development. *Tectonophysics* **16**, 1-46.

IRELAND T. R., FLOTTMANN T., FANNING C. M., GIBSON G. M. & PREISS W. V. 1998. Development of the early Paleozoic Pacific margin of Gondwana from detrital-zircon ages across the Delamerian orogen. *Geology* **26**, 243-246.

JAGO J. B., GUM J. C., BURTT A. C. & HAINES P. W. 2003. Stratigraphy of the Kanmantoo Group: a critical element of the Adelaide Fold Belt and the Palaeo-Pacific plate margin, Eastern Gondwana. *Australian Journal of Earth Sciences* **50**, 343-363.

JAMES P. R. & CLARK I. F. (Editors) 2002. *Geology* (2nd edition). (The Natural History of Kangaroo Island). Royal Society of South Australia.

JENKINS R. J. F. & SANDIFORD M. 1992. Observations on the tectonic evolution of the southern Adelaide Fold Belt. *Tectonophysics* **214**, 27-36.

KELSEY D. E., WADE B. P., COLLINS A. S., HAND M., SEALING C. R. & NETTING A. 2008. Discovery of a Neoproterozoic basin in the Prydz belt in East Antarctica and its implications for Gondwana assembly and ultrahigh temperature metamorphism. *Precambrian Research* **161**, 355-388.

KIRKLAND C. L., SPAGGIARI C. V., PAWLEY M. J., WINGATE M. T. D., SMITHIES R. H., HOWARD H. M., TYLER I. M., BELOUSOVA E. A. & POUJOL M. 2011. On the edge: U-Pb, Lu-Hf, and Sm-Nd data suggests reworking of the Yilgarn craton margin during formation of the Albany-Fraser Orogen. *Precambrian Research* **187**, 223-247.

KLEPEIS K. A., CRAWFORD M. L. & GEHRELS G. 1998. Structural history of the crustal-scale Coast shear zone north of Portland Canal, southeast Alaska and British Columbia. *Journal of Structural Geology* **20**, 883-904.

LEISS B., ULLEMEYER K., WEBER K., BROKMEIER H. G., BUNGE H. J., DRURY M., FAUL U., FUETEN F., FRISCHBUTTER A., KLEIN H., KUHS W., LAUNEAU P., LLOYD G. E., PRIOR D. J., SCHEFFZÜK C., WEISS T., WALTHER K. & WENK H. R. 2000. Recent developments and goals in texture research of geological materials. *Journal of Structural Geology* **22**, 1531-1540.

LI Z. X., BOGDANOVA S. V., COLLINS A. S., DAVIDSON A., DE WAELE B., ERNST R. E., FITZSIMONS I. C. W., FUCK R. A., GLADKOCHUB D. P., JACOBS J., KARLSTROM K. E., LU S., NATAPOV L. M., PEASE V., PISAREVSKY S. A., THRANE

K. & VERNIKOVSKY V. 2008. Assembly, configuration, and break-up history of Rodinia: A synthesis. *Precambrian Research* **160**, 179-210.

LLOYD G. E. 1987. Atomic number and crystallographic contrast images with the SEM: a review of backscattered electron techniques. *mineralogical magazine* **51**, 3-19.

LLOYD G. E. & FERGUSON C. C. 1986. A spherical electron-channelling pattern map for use in quartz petrofabric analysis. *Journal of Structural Geology* **8**, 517-526.

LLOYD G. E. & FREEMAN B. 1991. SEM electron channelling analysis of dynamic recrystallization in a quartz grain. *Journal of Structural Geology* **13**, 945-953.

MACKTELOW N. S. (Editor) 1990. *The structure of the southern Adelaide Fold Belt, South Australia*. (The evolution of a late Precambrian-early Palaeozoic rift complex: The Adelaide Geosyncline.). Geological Society of Australia, Special Publication.

MANCKTELOW N. S. 1981. Variation in fold axis geometry and slaty cleavage microfabric associated with a major fold arc, Fleurieu Peninsula, South Australia. *Journal of the Geological Society of Australia* **28**, 1 - 12.

MARSHAK S. 1988. Kinematics of Orocline and Arc Formation in Thin-Skinned Orogens. *Tectonics* **7**, 73-86.

MARSHAK S. & FLÖTTMANN T. 1996. Structure and origin of the Fleurieu and Nackara Arcs in the Adelaide fold-thrust belt, South Australia: Salient and recess development in the Delamerian Orogen. *Journal of Structural Geology* **18**, 891-908.

OFFLER R. & FLEMING P. D. 1968. A synthesis of folding and metamorphism in the Mt Lofty Ranges, South Australia. *Journal of the Geological Society of Australia* **15**, 245 - 266.

PASSCHIER C. W. & TROUW R. A. J. 2005. *Mircotectonics* (2nd edition). Springer-Verlag, Berlin.

PAULI C., SCHMID S. M. & HEILBRONNER R. P. 1996. Fabric domains in quartz mylonites: localized three dimensional analysis of microstructure and texture. *Journal of Structural Geology* **18**, 1183-1203.

PAYNE J. L., HAND M., BAROVICH K. M. & WADE B. P. 2008. Temporal constraints on the timing of high-grade metamorphism in the northern Gawler Craton: implications for assembly of the Australian Proterozoic. *Australian Journal of Earth Sciences: An International Geoscience Journal of the Geological Society of Australia* **55**, 623 - 640.

PLATT J. P. & BEHRMANN J. H. 1986. Structures and fabrics in a crustal-scale shear zone, Betic Cordillera, SE Spain. *Journal of Structural Geology* **8**, 15-33.

POWELL C. M., PREISS W. V., GATEHOUSE C. G., KRAPEZ B. & LI Z. X. 1994. South Australian record of a Rodinian epicontinental basin and its mid-neoproterozoic breakup (~700 Ma) to form the Palaeo-Pacific Ocean. *Tectonophysics* **237**, 113-140.

PREISS W. V. 2000. The Adelaide Geosyncline of South Australia and its significance in Neoproterozoic continental reconstruction. *Precambrian Research* **100**, 21-63.

PRIOR D. J., BOYLE A. P., BRENKER F., CHEADLE M. C., DAY A., LOPEZ G., PERUZZI L., POTTS G., REDDY S., SPIESS R., TIMMS N. E., TRIMBY P., WHEELER J. & ZETTERSTROM L. 1999. The application of electron backscatter diffraction and orientation contrast imaging in the SEM to textural problems in rocks. *American Mineralogist* **84**, 1741-1759.

RAIMONDO T., COLLINS A. S., HAND M., WALKER-HALLAM A., SMITHIES R. H., EVINS P. M. & HOWARD H. M. 2009. Ediacaran intracontinental channel flow. *Geology* **37**, 291-294.

RAIMONDO T., COLLINS A. S., HAND M., WALKER-HALLAM A., SMITHIES R. H., EVINS P. M. & HOWARD H. M. 2010. The anatomy of a deep intracontinental orogen. *Tectonics* **29**, TC4024.

SANDIFORD M., FODEN J., SHAOHUA Z. & TURNER S. 1992. Granite genesis and the mechanics of convergent orogenic belts with application to the southern Adelaide Fold Belt. *Transactions - Royal Society of Edinburgh: Earth Sciences* **83**, 83-93.

SANDIFORD M., OLIVER R. L., MILLS K. J. & ALLEN R. V. 1990. A cordierite-staurolite-muscovite association, east of Springton, Mt Lofty Ranges; implications for the metamorphic evolution of the

Kanmantoo Group. *The evolution of a late Precambrian-early Palaeozoic rift complex: the Adelaide geosyncline*, 483-495.

SCHMID S. M. & CASEY M. 1986. Complete fabric analysis of some commonly observed quartz c-axis patterns in In: Hobbs, B.E., Heard, H.C. (Eds.), Mineral and Rock Deformation: Laboratory Studies *American Geophysical Union*, 246-261.

SCHMIDT N.-H. & OLESEN N. O. 1989. Computer-aided determination of crystal-lattice orientation from electron channeling patterns in the SEM. *Can Mineral* **27**, 15-22.

SMITHIES R. H., HOWARD H. M., EVINS P. M., KIRKLAND C. L., KELSEY D. E., HAND M., WINGATE M. T. D., COLLINS A. S. & BELOUSOVA E. 2011. High-temperature granite magmatism, crust-mantle interaction and the mesoproterozoic intracontinental evolution of the Musgrave Province, Central Australia. *Journal of Petrology* **52**, 931-958.

SQUIRE R. J., CAMPBELL I. H., ALLEN C. M. & WILSON C. J. L. 2006. Did the Transgondwanan Supermountain trigger the explosive radiation of animals on Earth? *Earth and Planetary Science Letters* **250**, 116-133.

TOY V. G., PRIOR D. J. & NORRIS R. J. 2008. Quartz fabrics in the Alpine Fault mylonites: Influence of pre-existing preferred orientations on fabric development during progressive uplift. *Journal of Structural Geology* **30**, 602-621.

TURNER S., FODEN J., SANDIFORD M. & BRUCE D. 1993. Sm-Nd isotopic evidence for the provenance of sediments from the Adelaide Fold Belt and southeastern Australia with implications for episodic crustal addition. *Geochimica et Cosmochimica Acta* **57**, 1837-1856.

VAN ACHTERBERGH E., RYAN C. G., JACKSON S. E. & GRIFFIN W. L. 2001. Data reduction software for LA-ICP-MS. *In:* Sylvester P. J. ed., *Laser-ablation-ICPMS in the earth sciences; principles and applications.*, Mineralogical Association of Canada. Ottawa, ON, Canada. 2001.

VEEVERS J. J. 2006. Updated Gondwana (Permian–Cretaceous) earth history of Australia. *Gondwana Research* **9**, 231-260.

VEEVERS J. J. 2007. Pan-Gondwanaland post-collisional extension marked by 650–500 Ma alkaline rocks and carbonatites and related detrital zircons: A review. *Earth-Science Reviews* **83**, 1-47.

VEEVERS J. J., BELOUSOVA E. A., SAEED A., SIRCOMBE K., COOPER A. F. & READ S. E. 2006. Pan-Gondwanaland detrital zircons from Australia analysed for Hf-isotopes and trace elements reflect an ice-covered Antarctic provenance of 700–500 Ma age, TDM of 2.0–1.0 Ga, and alkaline affinity. *Earth-Science Reviews* **76**, 135-174.

VEEVERS J. J. & SAEED A. 2007. Central Antarctic provenance of Permian sandstones in Dronning Maud Land and the Karoo Basin: Integration of U-Pb and TDM ages and host-rock affinity from detrital zircons. *Sedimentary Geology* **202**, 653-676.

VEEVERS J. J. & SAEED A. 2008a. Gamburtsev Subglacial Mountains provenance of Permian-Triassic sandstones in the Prince Charles Mountains and offshore Prydz Bay: Integrated U-Pb and TDM ages and host-rock affinity from detrital zircons. *Gondwana Research* **14**, 316-342.

VEEVERS J. J. & SAEED A. 2008b. Gamburtsev Subglacial Mountains provenance of Permian–Triassic sandstones in the Prince Charles Mountains and offshore Prydz Bay: Integrated U–Pb and TDM ages and host-rock affinity from detrital zircons. *Gondwana Research* **14**, 316-342.

VEEVERS J. J., SAEED A. & O'BRIEN P. E. 2008a. Provenance of the Gamburtsev Subglacial Mountains from U-Pb and Hf analysis of detrital zircons in Cretaceous to Quaternary sediments in Prydz Bay and beneath the Amery Ice Shelf. *Sedimentary Geology* **211**, 12-32.

VEEVERS J. J., SAEED A., PEARSON N., BELOUSOVA E. & KINNY P. D. 2008b. Zircons and clay from morainal Permian siltstone at Mt Rymill (73°S, 66°E), Prince Charles Mountains, Antarctica, reflect the ancestral Gamburtsev Subglacial Mountains–Vostok Subglacial Highlands complex. *Gondwana Research* **14**, 343-354.

VON DER BORCH C. C. 1980. Evolution of late proterozoic to early paleozoic Adelaide foldbelt, Australia: Comparisons with postpermian rifts and passive margins. *Tectonophysics* **70**, 115-134.

WANG Y., LIU D., CHUNG S.-L., TONG L. & REN L. 2008. SHRIMP zircon age constraints from the Larsemann Hills region, Prydz Bay, for a late Mesoproterozoic to early Neoproterozoic tectono-thermal event in East Antarctica. *Am J Sci* **308**, 573-617.

WEIL A. B., YONKEE A. & SUSSMAN A. 2010. Reconstructing the kinematic evolution of curved mountain belts: A paleomagnetic study of Triassic red beds from the Wyoming salient, Sevier thrust belt, USA. *Geological Society of America Bulletin* **122**, 3-23.

WYSOCZANSKI R. J. & ALLIBONE A. H. 2004. Age, Correlation, and Provenance of the Neoproterozoic Skelton Group, Antarctica: Grenville Age Detritus on the Margin of East Antarctica. *Journal of Geology* **112**, 401-416.

YASSAGHI A., JAMES P. R. & FLÖTTMANN T. 2000. Geometric and kinematic evolution of asymmetric ductile shear zones in thrust sheets, southern Adelaide Fold-Thrust Belt, South Australia. *Journal of Structural Geology* **22**, 889-912.

YASSAGHI A., JAMES P. R., FLÖTTMANN T. & WINSOR C. N. 2004. P-T conditions and kinematics of shear zones from the southern Adelaide Fold-Thrust Belt, South Australia: insights into the dynamics of a deeply eroded orogenic wedge. *Australian Journal of Earth Sciences* **51**, 301-317.

TABLES

Table 1- Shows sample names, locations and descriptions of the units they were taken from. Also shows the techniques used on each sample and the youngest U-Pb grain and maximum depositional ages found in these samples.

Table 2- Provided descriptions of zircons found in samples used for U-Pb laser ICPMS

Table 3- Gives a summary of Electron backscatter diffraction (EBSD) results including sample name, relative mineral lineations and foliations, degree of indexing, patterns found on stereographic plots and potential slip-systems.

Table 4- Gives a list of orientations and structures found on seismic line interpretations.

FIGURE CAPTIONS

Figure 1-

(a)The South Australian Fold Belt showing major sedimentary stratigraphy and cratonic basement. The fold belt can be divided into 3 areas, the Fleurieu Arc, the Transitional Domain and the Narkar Arc. Adapted from (Flöttmann & James 1997). Stars indicate transect locations. (b) The Orientation of the SAFTB in relation to Antarctica and the Ross-Delamerian Orogenies in East Gondwana *ca* 520 Ma. The Gawler Craton is also highlighted. Adapted from (Foden *et al.* 2006; Veevers 2006; Veevers *et al.* 2006; Haines *et al.* 2009; Boger 2011)

Figure 2-

Kangaroo Island showing the platform rocks of the KI group, The Kanmantoo Group sediments and the Kangaroo Island Shear Zone. Delamerian related structures and granites are indicated in black. Adapted from (Flöttmann *et al.* 1995; Flöttmann & James 1997; Flöttmann *et al.* 1998)

Figure 3-

Simplified Stratigraphy of the Adelaide Basin (Preiss 2000), Kanmantoo Basin (Daily *et al.* 1979; Macktelow 1990; Flöttmann *et al.* 1994; Belperio 1995; Flöttmann *et al.* 1998; Haines *et al.* 2001; Jago *et al.* 2003) and Kangaroo Island Platform (Daily *et al.* 1979; Daily *et al.* 1980; Macktelow 1990; Flöttmann *et al.* 1995; Flöttmann & Cockshell 1996) showing previous work undertaken on certain sections. <z> indicates U-Pb zircon dating (Ireland *et al*. 1998). (m) indicated Detrital muscovite dating(Haines *et al*. 2004). @ indicates Sm-Nd isotopic Studies (Turner *et al*. 1993). # indicates geochemistry and Nd-isotopic studies (Haines *et al*. 2009).

Figure 4-

Bathymetry Map of Kangaroo Island and the Fleurieu Peninsular (PIRSA) overlain with the seismic lines used in this study. Orientations of these lines are found in Table 3.

Figure 5-

Seismic line 94SME-12 running SSE-NNW across the page with faults interpreted in blue and the base of the Cambrian in pink. Black box indicates the expected orientation on the KIFPSZ on this line.

Figure 6-

Seismic line 92-13 running SE-NW across the page with faults interpreted in blue and the base of the Cambrian in pink. Black box indicates the expected orientation on the KIFPSZ on this line.

Figure 7-

Seismic line 92DME-1 running NW-SE across the page faults interpreted in blue and the base of the Cambrian in pink.

Figure 8-

Seismic line MESA96-1 NW-SE across the page faults interpreted in blue and the base of the Cambrian in pink. Black box indicates the expected orientation on the KIFPSZ on this line.

Figure 9-

Legend used for strain logs in Figures 11, 14 and 16

Figure 10-

Large Map of transect along the Port Morrison Area, Kangaroo Island, South Australia

Figure 11-

Compilation of data from Port Morrison a) a zoomed in section of the 2 km detailed transect line A-B indicates the location of the Strain Log. b) Strain Log along the Point Morrison section across line A-B. In order to highlight varying degrees of shear, the degree of bedding present verse the degree of shear foliation present is used. The mid-point on this scale is when one fabric become more pervasive, than the dominate fabric. c) Map of transect Along the Port Morrison Area, Kangaroo Island, South Australia.

Figure 12-

Outcrop images from Point Morrison with annotations the black arrows are pointing North in all images; a) shows decimetre sized asymmetric folds with the axial plunge shown with a blue arrow and the axial plane with a dashed red line. b) shows the overturned cross-bedding that indicates younging to the north. c)Folding of quartz thick quartz rich layers in-between finer grained pelitic sections. Axial plunges are shown with a blue arrow and the axial planes with a dashed red line. d) a thick, more rigid quartz layer with finer bedded, more ductile pelitic layers that are forming small scale folds. These folds have been truncated by the more rigid layer.

Figure 13-

Large Map of transect Along the Snugg Cove Area, Kangaroo Island, South Australia

Figure 14-

Compilation of data from Snugg Cove a) a zoomed in section of the detailed transect line A-B indicates the location of the Strain Log. Line C-D indicated the orientation of annotated image b). b) Shows the Southern outcrop at Snugg Cove; the changes in Domain 2 and 3 can be seen

along the cliff face Line C-D. c) Strain Log along the Snugg Cove section across line A-B. In order to highlight varying degrees of shear, the degree of bedding present verse the degree of shear foliation present is used. The mid-point on this scale is when one fabric become more pervasive, of the dominate fabric.

Figure 15-

Outcrop images From Snugg Cove with annotations the black arrows are pointing North in all images; a) σ-clast of a quartz boudins from the southern part of Domain 2, near the Doman 3 boundary showing top to the north transport direction. b) δ-clast showing wrap-around tails from Domain 2, indicating top to the north-west displacement. c) From Domain 2, decimetres thick sandstone beds that have been faulted and infilled with quartz. The muscovite rich layers are wrapping around the more brittlely deformed sandstone bed. d) On the edge of Domain 2 and 3; metre-scale thrust (annotated in grey) within an increasingly pelitic rock, that has muscovite rich layers and quartz boudins. e) A fold has developed within the less pelitic northern edge of Domain 2. There is a fault forming along the Axial plane of this fold. f) moving from left to right these images highlight outcrop changes along the Snugg Cover Section. Bedded and cleaved rocks in Domain 1 to sandstone and muscovite inter-bedding rocks in Domain 2 to increasingly muscovite rich, and quartz boudin rich areas at the end of Domain 2. The final picture shows then highly sheared, quartz-boudin rich rocks outcropping in Domain 3.

Figure 16-

Compilation of data from Little Gorge a) Strain Log along the Litte Gorge section across line A-B. In order to highlight varying degrees of shear, the degree of bedding present verse the degree of shear foliation present is used. As there are areas dominated by unbedded basement, low strain

and high strain have also been used in this log. The mid-point on this scale is when one fabric become more pervasive, of the dominate fabric. b) Map of transect Along the Little Gorge Area, Fleurieu Peninsula, South Australia. Line A-B indicates the location of the Strain Log.

Figure 17-

Outcrop images with annotations the black arrows are pointing North in all images; a) Overturned cross-bedding along the western edge of the shear zone that indicates younging to the north. b) C-S fabrics found along the base of large easterly cliffs. c) C-prime (C`) fabrics (dashed red lines) found within pelitic layers that are wrapping about metre-scale quartz boudins. d) highly sheared leucosome of potassium feldspar and quartz found 200 metres east, into the gorge. e) Part of the ten metre unit of coarse conglomerates and lithic arenites found east of the eroded limestone and cross bedded unit. f) outcropping rocks along the coast at the Little Gorge section show cross-bedded arenites.

Figure 18-

U-Pb data from ASKI11-08 a) shows a probability density plot for the 142 analyses carried out, with 44 being between 90-110% concordant. The red peaks indicate the concordant data with the blue peaks indicating all data. Significant populations were found at Ca 550-600 Ma and Ca 1000-1250 Ma. b) Conventional U-Pb Concordia plots for all zircon analyses from ASKI11-08. c) Cathodoluminecence images of representative zircons showing zonation and where analyses were undertake. Spot 42 gave the youngest concordant age for this sample; 556 ±19Ma.

Figure 19

U-Pb data from ASKI11-12 a) shows a probability density plot for the 132 analyses carried out with 61 being between 90-110% concordant. The red peaks indicate the concordant data with the blue peaks indicating all data. Significant populations were found at *ca* 600-700 Ma and *ca* 1000-1250 Ma. b) Conventional U-Pb Concordia plots for all zircon analyses from ASKI11-12. c) Cathodoluminecence images of representative zircons showing zonation and where analyses were undertake. Spot 35 gave the youngest concordant age for this sample; 546 ±7 Ma

Figure 20

U-Pb data from ASKI11-04 a) shows a probability density plot for the 89 analyses carried out with 33 being between 90-110% concordant. The red peaks indicate the concordant data with the blue peaks indicating all data. Significant populations were found at *ca* 550-600 Ma and *ca* 1000-1300 Ma. b) Conventional U-Pb Concordia plots for all zircon analyses from ASKI11-##. c) Cathodoluminecence images of representative zircons showing zonation and where analyses were undertake. Spot 143 gave the youngest concordant age for this sample; 547±7Ma

Figure 20-

Probability density plot comparisons; a) Shows a collation of U-Pb zircon ages for potential sources found in Antarctica coupled with all data from this study on the Kanmantoo Group Sedimentary rocks. Displayed as Probabilty deinsity plots with red bars indicating the youngest peak ca 500-700 Ma and the yellow line indicating the other significant peak ca 900-1300 Ma. Data after the following papers for the following areas: Prydz Bay (Kelsey *et al.* 2008; Veevers *et al.* 2008a); Eastern Antarctica (Goodge *et al.* 2002; Wysoczanski & Allibone 2004; Wang *et al.* 2008); Central Antarctica (Veevers & Saeed 2007; Elliot & Fanning 2008; Goodge *et al.*

2008); Prince Charles Mountains (Veevers & Saeed 2008a; Veevers *et al.* 2008b). The bottom graph shows a combination of the most likely sources with a dashed black line, indicating the Kanmantoo zircon age signature. b) Probability density plot comparisons of the three samples from this study, with all the data combined. Red bars indicating the youngest peak ca 500-700 Ma and the yellow line indicating the other significant peak ca 900-1300 Ma and highlight similar age spectra for all three samples.

Figure 21-

Stereographic data plots of quartz <c> axis (0001) and <a> axes (11-20) obtained thought Electron Backscatter Diffraction analysis. Images are plotted with the HKL CHANNEL 5 software package "Mambo" pole plotting application. Contours are composed using 24° half width and 5° data clustering. From top to bottom the samples run ASKI11-03, ASKI11-04, ASKI11-05, ASKI11-06, ASKI11-12. For descriptions of sample orientations and patterns see Table 3. For descriptions of location and lithology see Table 1.

Figure 22- a) shows orientation and movement along the relevant slip systems adapted from (Passchier & Trouw 2005). b) 1. Flinn diagram showing the relation of geometry of LPO patterns of quartz c-axes (*grey contours*) and a-axes (*striped ornament*) with strain in the case of coaxial progressive deformation. An inset shows the orientation of principal strain axes in the pole diagrams. *Horizontal solid lines* in pole diagrams indicate reference foliation. *Dots* indicate reference lineation (Passchier & Trouw 2005). b) 2. An orientation showing how shear sense can be inferred (Passchier & Trouw 2005). b) 3. Orientation of a quartz crystal in a reference frame defined by a foliation (Sr), lineation (Lr) and foliation pole showing <c> -axis and <a> -axes

(Passchier & Trouw 2005). c) Shows correlation between locations of c-axis peaks on CPO figures and the active slip systems in quartz (Schmid & Casey 1986; Toy *et al.* 2008). X is the lineation direction, Z the pole to foliation. This diagram has <c>-axis stereographic plots draped over the top to highlight the slip-systems active in samples from the KIFPSZ

Figure 23-

The Orientation of the Australian relation to Antarctica and the Ross-Delamerian Orogenies in East Gondwana *ca* 520 Ma, with potiential source areas highlighted and paleo-flow diffection for sections of Antarctica and South-eastern Australia (Haines *et al.* 1996; Flöttmann *et al.* 1998; Haines *et al.* 2001; Veevers & Saeed 2008a). Addapted from (Ireland *et al.* 1998; Hand & Sandiford 1999; Boger & Miller 2004; Veevers & Saeed 2008a; Haines *et al.* 2009; Boger 2011; Kirkland *et al.* 2011; Smithies *et al.* 2011).

Figure 24-

Shows temporal evolution of the Syn-orogenic nature of the Fleurieu Arc section of the SAFTB adapted from (Macktelow 1990; Belperio & Flint 1992; Jenkins & Sandiford 1992; Marshak & Flöttmann 1996) combined with schematic diagrams of how syn-orogenic curves can form (Marshak 1988; Marshak & Flöttmann 1996; Costa & Speranza 2003; Weil *et al.* 2010).

Figure 25-

Fault reactivation diagrams for averaged shear zone readings along the KIFPSZ indicate that regardless of the stress field, the orientation of this structure is highly likely to be reactivated.

Sample	Locations	Description	U-Pb	Youngest Grain	Maximum Dep. Age	EBSD
ASKI11-03	Point Morrison, Northern Edge of the Large Shear Zone	Quartz rich phyllite layer from within strained, interbedded shale layer	No			Yes
ASKI11-04	Point Morrison, Southern Edge of the Large Shear Zone	Quartz rich phyllite layer from within strained, interbedded shale layer	Yes	574± 7 Ma	623 ± 31 Ma	Yes
ASKI11-05	Snugg Cove, Southern Section of Domain 2	Quartz rich layer from an area that is sandstone rich with interbedded fine muscovite roch layers	No			Yes
ASKI11-06	Snugg Cove, Domain 3	Quartz rich layer within a more pelitic area that looks more strained which is rich in muscovite and biotite rich	No			Yes
ASKI11-08	Snugg Cove, Domain 3	muscovite rich layer within pelitic, muscovite rich area	Yes	556±19 Ma	587±17 Ma	No
ASKI11-12	Snugg Cove, Nothern Section of Domain 2	Quartz rich sandstone layer within a muscovite rich section	Yes	546±7 Ma	617± Ma	Yes

Table 1

Sample	Rock Unit	Size µm	Colour	Aspect ratio	Shape	CL descriptions
ASKI11-04	Deformed Kanmantoo, Point Morrison	40-90	yellow to colourless	1:2	Heterogeneous; equant and stubby to tabular and well developed	Small but well persevered oscillatory zoning and well developed sector zoning. Some zoned grains have xenocrystic cores with areas of localised resorbtion
ASKI11-08	Deformed Kanmantoo, Snugg Cove	30-85	yellow to colourless	1:2	Shapes are present ranging from equant to tabular, with a higher abundance of tabular grains	Equant grains have thick rims though a number show sections of resorbtion, some cores also show alteration and resorbtion
ASKI11-12	Deformed Kanmantoo, Snugg Cove	60-200	yellow to colourless	1:3	Tabular crystals have rounded edges and there is a mix of equant and elongate grains	Well preserved sector zoning, many of the equant grains showing cores with relic sector zoning and thick resorbed rims. with alterated rims

Table 2

Sample	Lineation	Foliation	Axes	co-axial V non-coaxial	Description of patters	Slip Systems
ASKI11-03	80→129	71/168	C-plane-0001	Non-coaxial	One girdle running diagonally from top LSH with a dominant high in the bottom RH corner	Rhomb <a> slip Prism <a> slip c-slip= high temperature
			A-plane-11-20	Non-coaxial	Two circular areas, one in the top LH corner, one off centre to the RHS. Smaller domains are on the edge of the bottom LHS and the top RHS	
ASKI11-04	60→131	64/185	C-plane-0001	Non-coaxial	One dominant concentration of poles orientated in the top RHS	Rhomb <a> slip
			A-plane-11-20		A patchy girdle that runs from the top LHS into the top RHS and down into the bottom RHS	
ASKI11-05	20→168	33/179	C-plane-0001	Coaxial	Two main girdles that run on either side of the diagram from the lower LHS up to the upper LHS and the lower RHS to the upper LHS	Cleft girdle = high temperature constructional strain
			A-plane-11-20		Two main girdles that run on either side of the diagram from the lower LHS up to the upper LHS and the lower RHS to the upper LHS.	
ASKI11-06	38→158	40/178	C-plane-0001	Non-coaxial	Two concentrations of points in the upper LH edge and the lower RH edge	c-slip = high temperature
			A-plane-11-20		One main population near centre of the diagram	
ASKI11-12	46→154	52/175	C-plane-0001	Non-coaxial	Three locations, two that dominate the upper LH side and one that dominates the bottom RH edge	c-slip = high temperature
			A-plane-11-20		A patchy girdle that runs from the top LHS into the centre and up into RH edge	Looks like one half of a flattening strain girdle; high T flattening strain

Table 3

Line	Line Orientation	Number Of Faults	Fault Plunge	Fold vergance	Transport Direction	Degree of shortening	Fault Style
92-13	SE-NW	4	SE	NW	Top→NW	Significant	Imbricate reverse faults
92DME-1	NW-SE	9	SE	NW	Top→NW	Significant	Duplex system with two other reverse faults
94DME-12	SSE-NNW	3	SSE	NWW	Top→NNW	Significant	Broadly spaced imbricate reverse faults
MESA96-1	NW-SE	5	SE	NW	Top→ NW	Significant	Imbricate reverse faults

Table 4

IMAGES

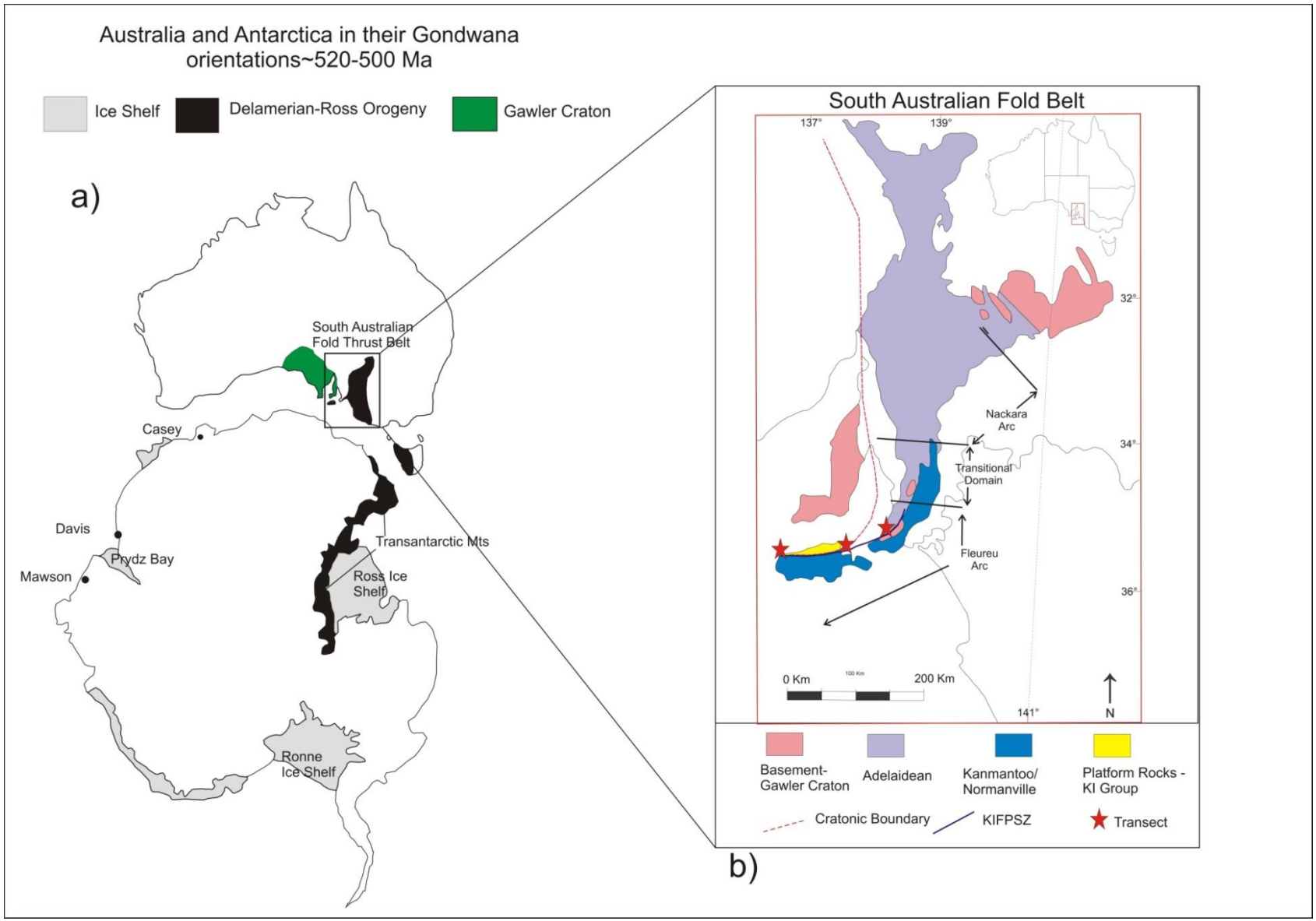
Australia and Antarctica in their Gondwana orientations~520-500 Ma
Ice Shelf
Delamerian-Ross Orogeny
Gawler Craton
a)
South Australian Fold Thrust Belt
Casey
Davis
Prydz Bay
Mawson
Transantarctic Mts
Ross Ice Shelf
Ronne Ice Shelf
South Australian Fold Belt
137°
139°
32°
34°
36°
141°
Nackara Arc
Transitional Domain
Fleureu Arc
0 Km
100 Km
200 Km
N
Basement-Gawler Craton
Adelaidean
Kanmantoo/ Normanville
Platform Rocks - KI Group
Cratonic Boundary
KIFPSZ
Transect
b)

Figure 1

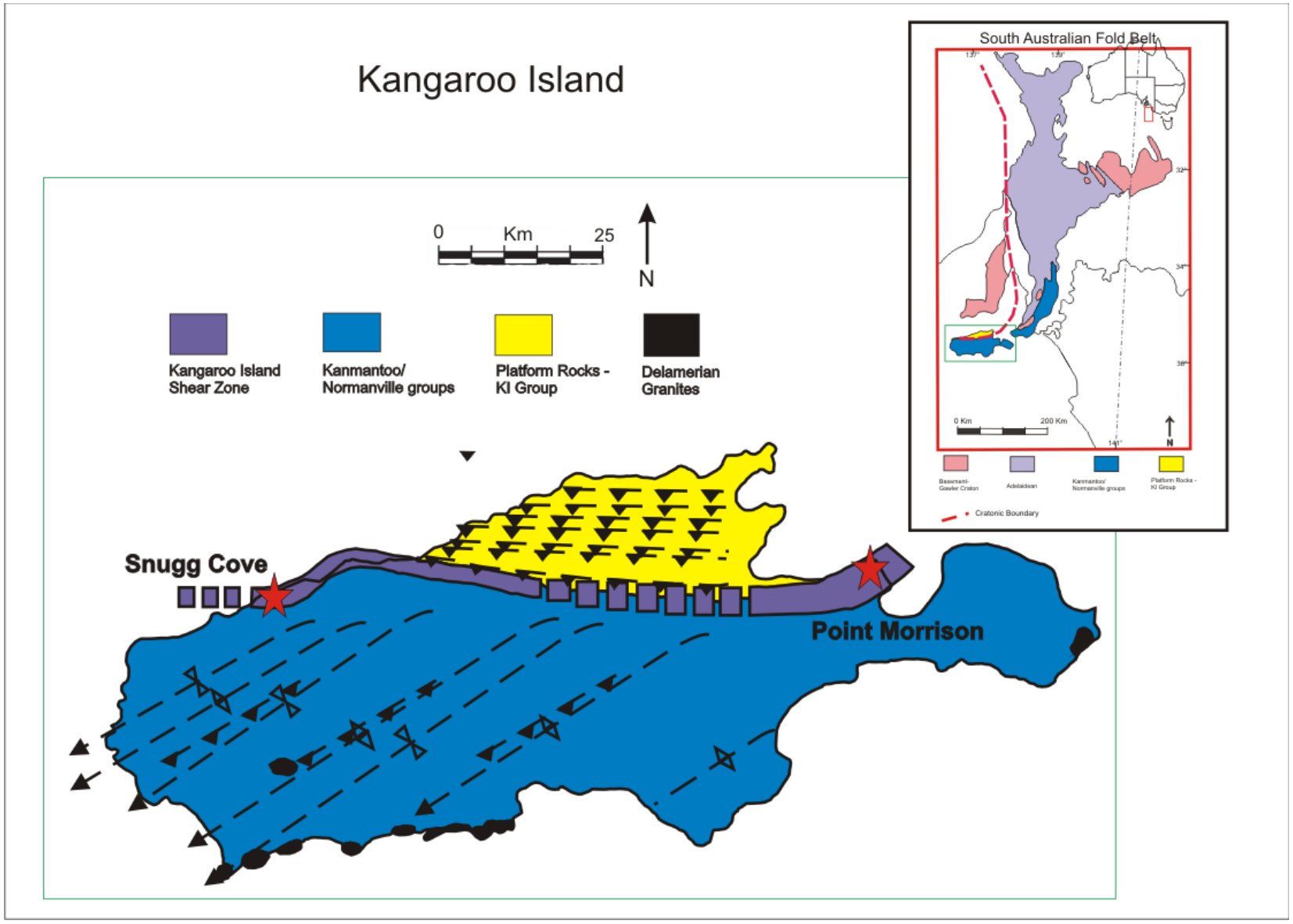
Kangaroo Island
0
Km
25
N
Kangaroo Island Shear Zone
Kanmantoo/ Normanville groups
Platform Rocks - KI Group
Delamerian Granites
Snugg Cove
Point Morrison
South Australian Fold Belt
0 Km
200 Km
N
Cratonic Boundary

Figure 2

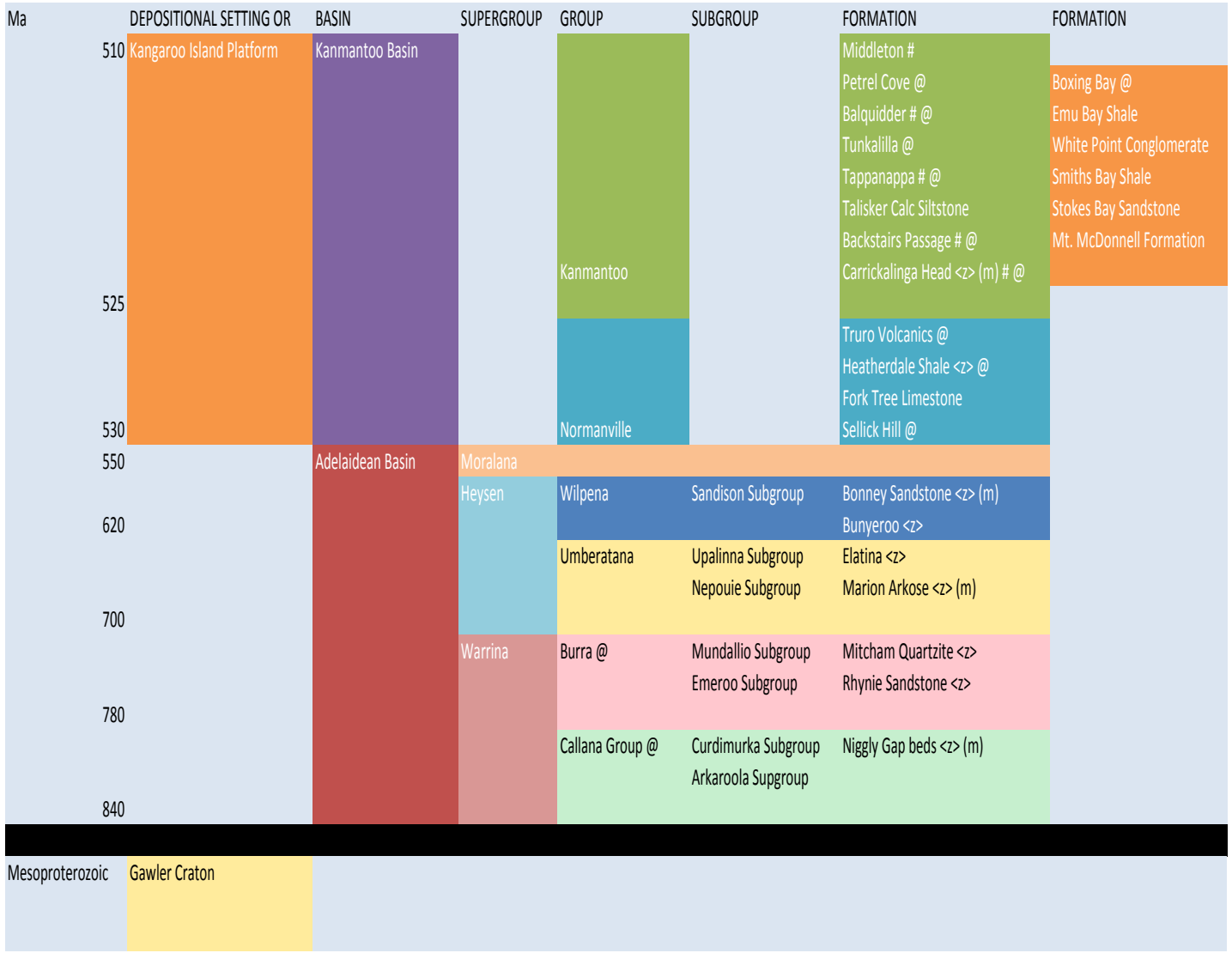
Ma
DEPOSITIONAL SETTING OR
BASIN
SUPERGROUP
GROUP
SUBGROUP
FORMATION
FORMATION
510
525
530
550
620
700
780
840
Kangaroo Island Platform
Kanmantoo Basin
Middleton #
Petrel Cove @
Balquidder # @
Tunkalilla @
Tappanappa # @
Talisker Calc Siltstone
Backstairs Passage # @
Carrickalinga Head <z> (m) # @
Boxing Bay @
Emu Bay Shale
White Point Conglomerate
Smiths Bay Shale
Stokes Bay Sandstone
Mt. McDonnell Formation
Kanmantoo
Truro Volcanics @
Heatherdale Shale <z> @
Fork Tree Limestone
Sellick Hill @
Normanville
Adelaidean Basin
Moralana
Heysen
Wilpena
Sandison Subgroup
Bonney Sandstone <z> (m)
Bunyeroo <z>
Umberatana
Upalinna Subgroup
Nepouie Subgroup
Elatina <z>
Marion Arkose <z> (m)
Warrina
Burra @
Mundallio Subgroup
Emeroo Subgroup
Mitcham Quartzite <z>
Rhynie Sandstone <z>
Callana Group @
Curdimurka Subgroup
Arkaroola Supgroup
Niggly Gap beds <z> (m)
Mesoproterozoic
Gawler Craton

Figure 3

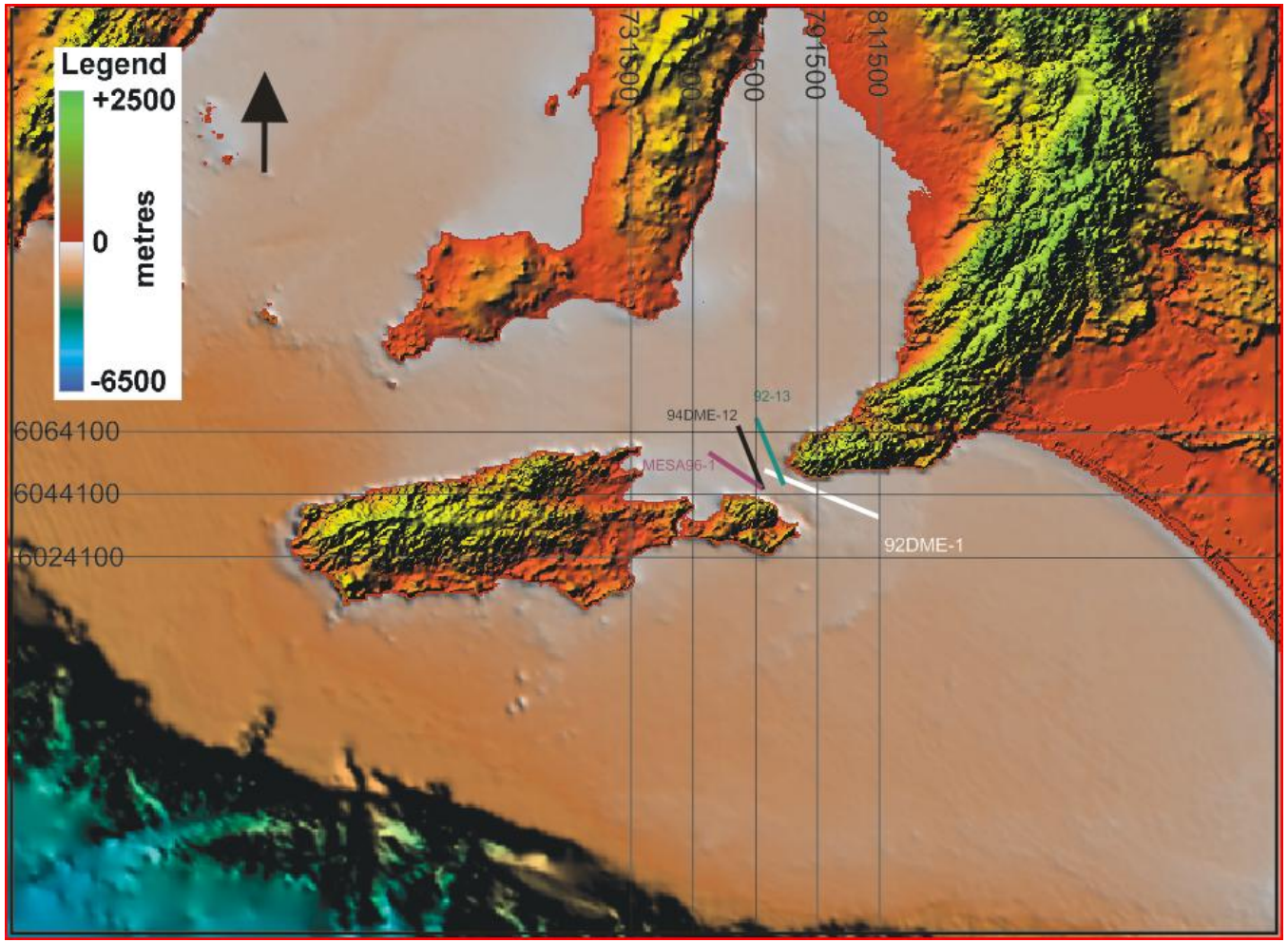
Legend
+2500
0
metres
-6500
731500
791500
811500
6064100
6044100
6024100
94DME-12
92-13
MESA96-1
92DME-1

Figure 4

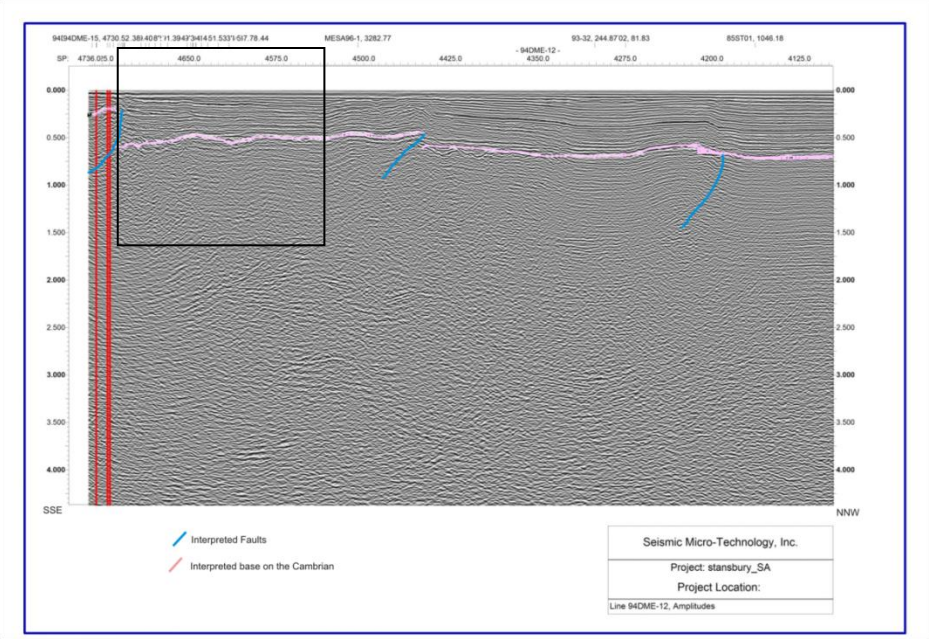

Figure 5

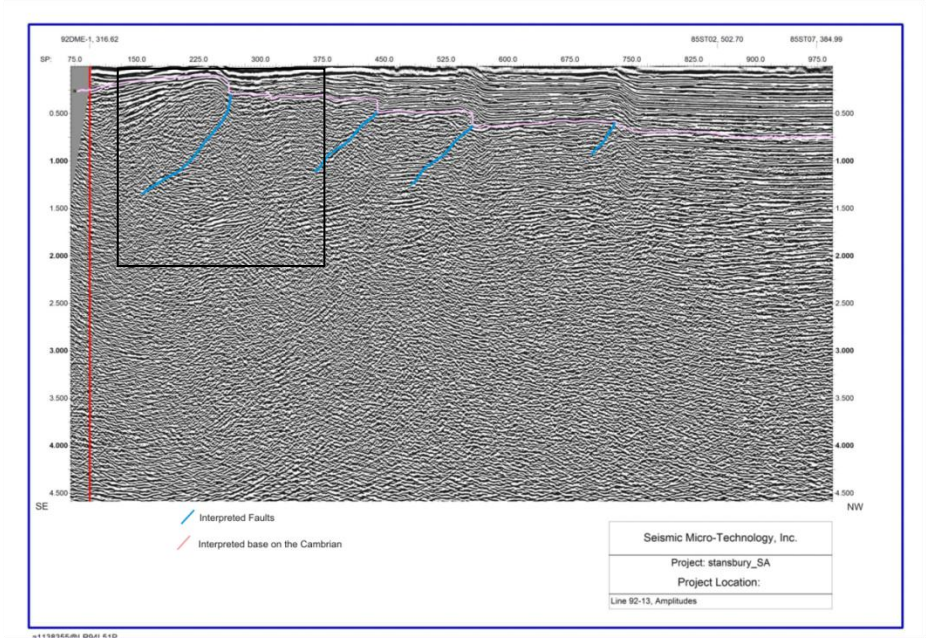

Figure 6

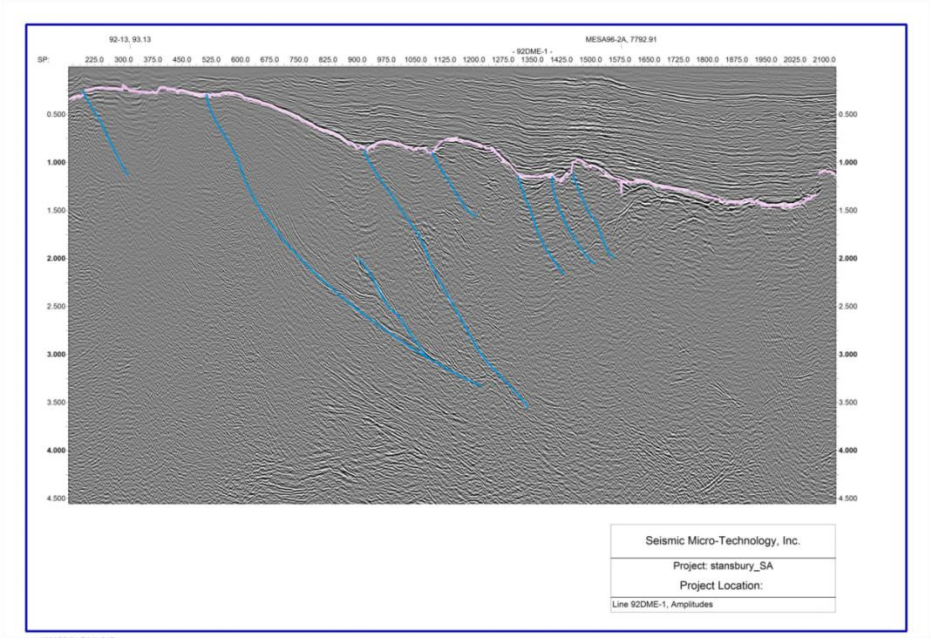

Figure 7

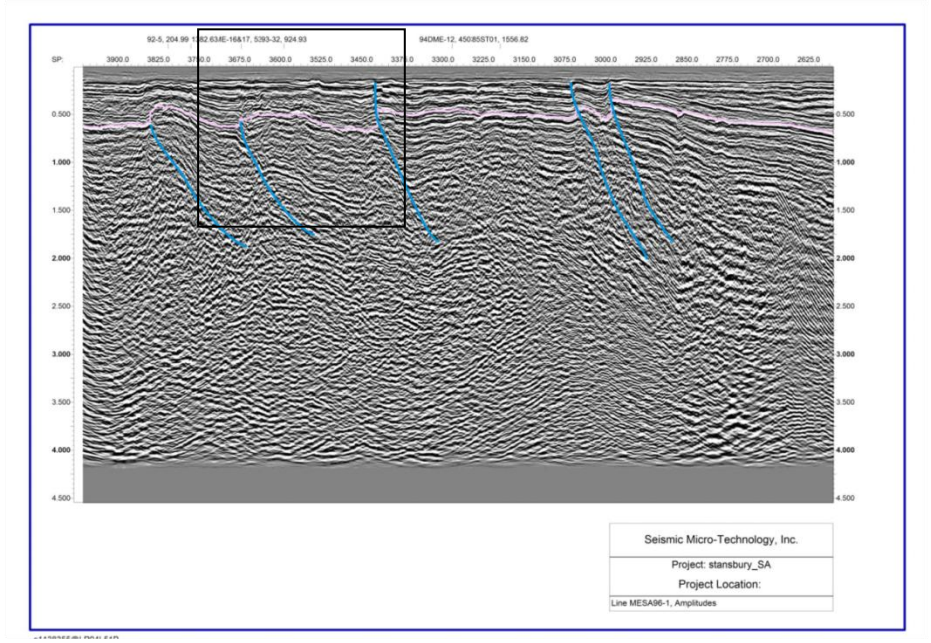

Figure 8

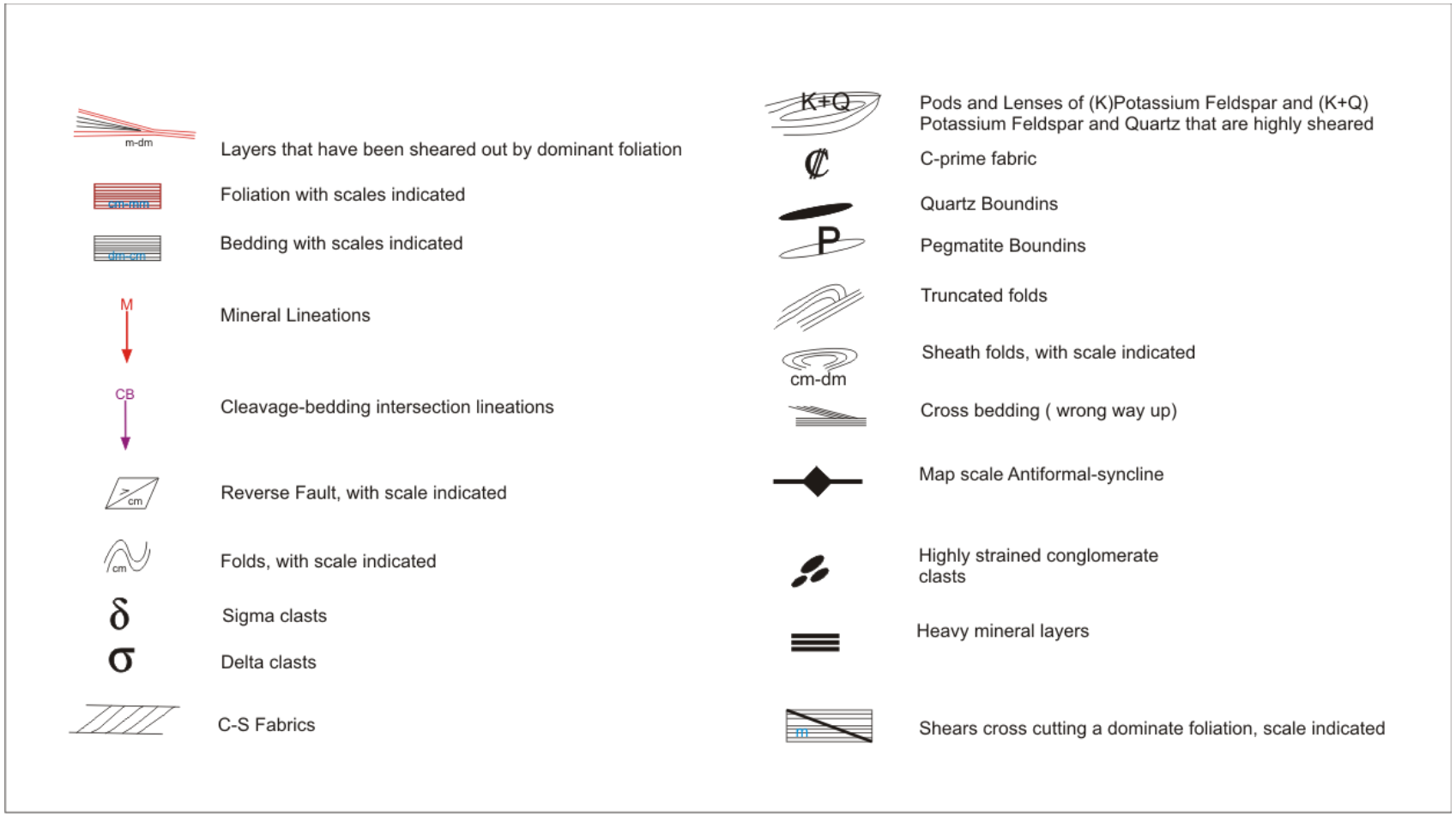
m-dm
Layers that have been sheared out by dominant foliation
cm-mm
Foliation with scales indicated
dm-cm
Bedding with scales indicated
M
Mineral Lineations
CB
Cleavage-bedding intersection lineations
> cm
Reverse Fault, with scale indicated
cm
Folds, with scale indicated
δ
Sigma clasts
σ
Delta clasts
C-S Fabrics
K+Q
Pods and Lenses of (K)Potassium Feldspar and (K+Q) Potassium Feldspar and Quartz that are highly sheared
C-prime fabric
Quartz Boundins
P
Pegmatite Boundins
Truncated folds
cm-dm
Sheath folds, with scale indicated
Cross bedding (wrong way up)
Map scale Antiformal-syncline
Highly strained conglomerate clasts
Heavy mineral layers
m
Shears cross cutting a dominate foliation, scale indicated

Figure 9

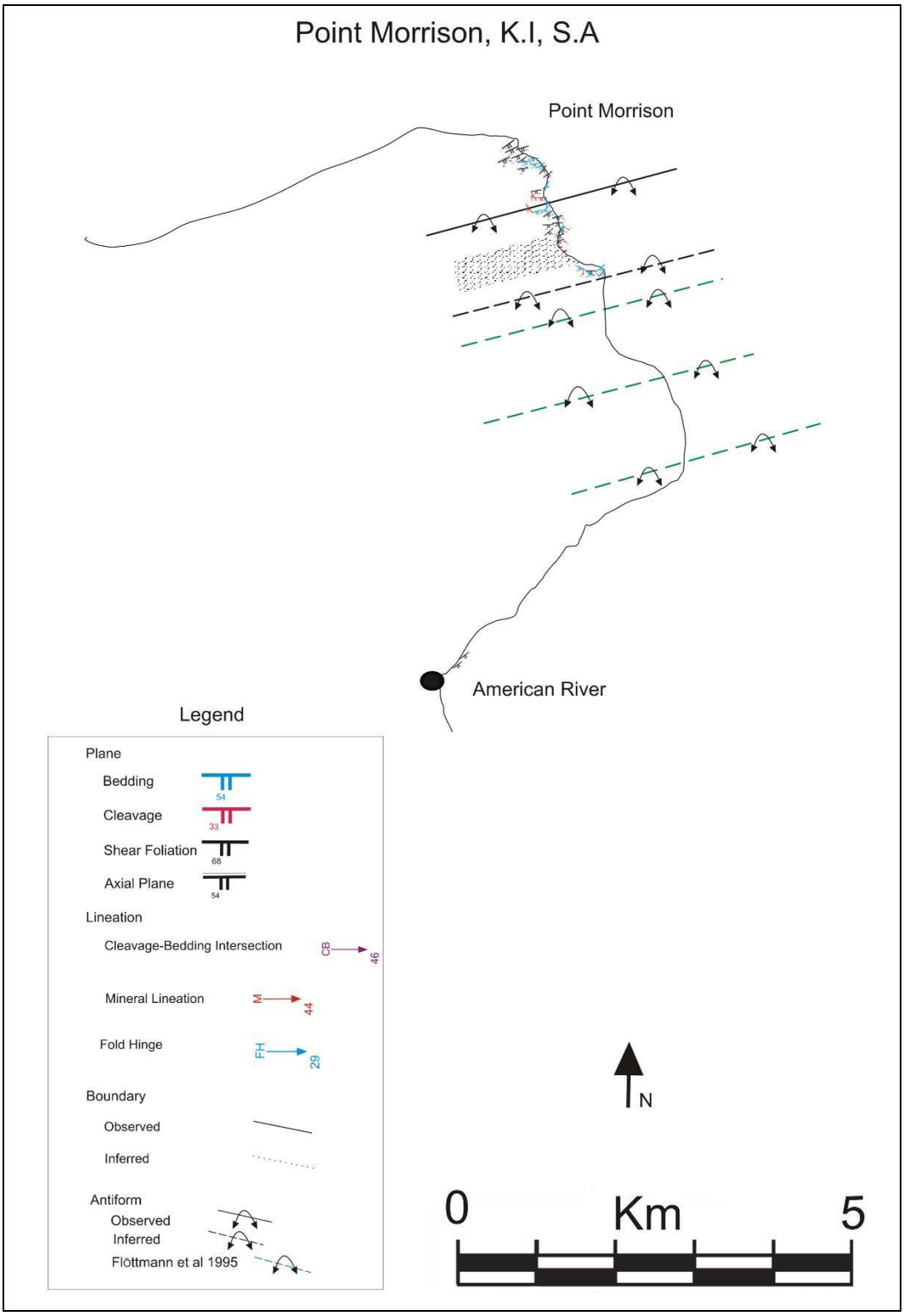
Point Morrison, K.I, S.A
Point Morrison
American River
Legend
Plane
Bedding
54
Cleavage
33
Shear Foliation
68
Axial Plane
54
Lineation
Cleavage-Bedding Intersection
CB
46
Mineral Lineation
M
44
Fold Hinge
FH
29
Boundary
Observed
Inferred
Antiform
Observed
Inferred
Flöttmann et al 1995
N
0
Km
5

Figure 10

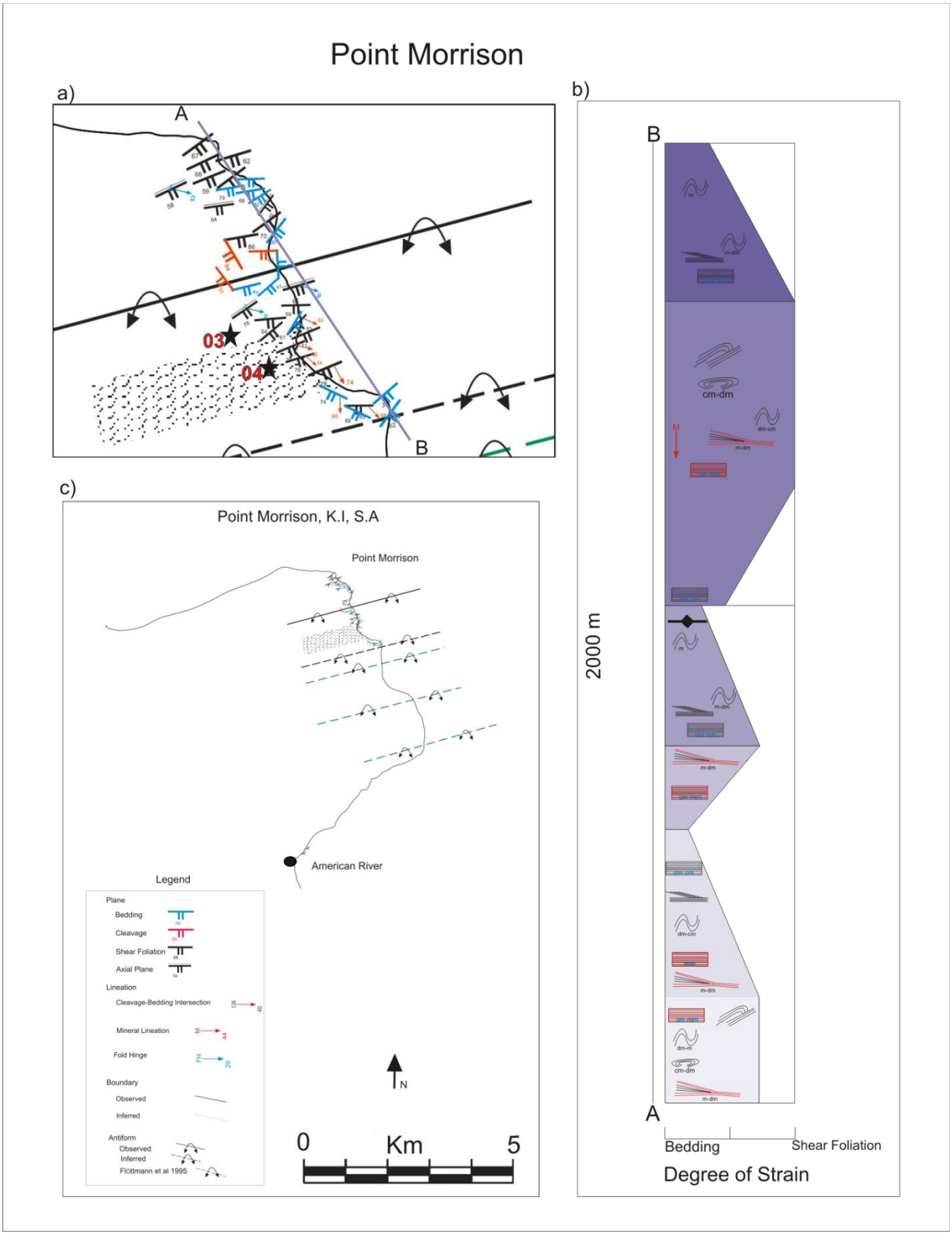
Point Morrison
a)
A
B
03
04
b)
B
A
2000 m
cm-dm
m-dm
dm-cm
Bedding
Shear Foliation
Degree of Strain
c)
Point Morrison, K.I, S.A
Point Morrison
American River
Legend
Plane
Bedding
Cleavage
Shear Foliation
Axial Plane
Lineation
Cleavage-Bedding Intersection
Mineral Lineation
Fold Hinge
Boundary
Observed
Inferred
Antiform
Observed
Inferred
Flottmann et al 1995
N
0
Km
5

Figure 11

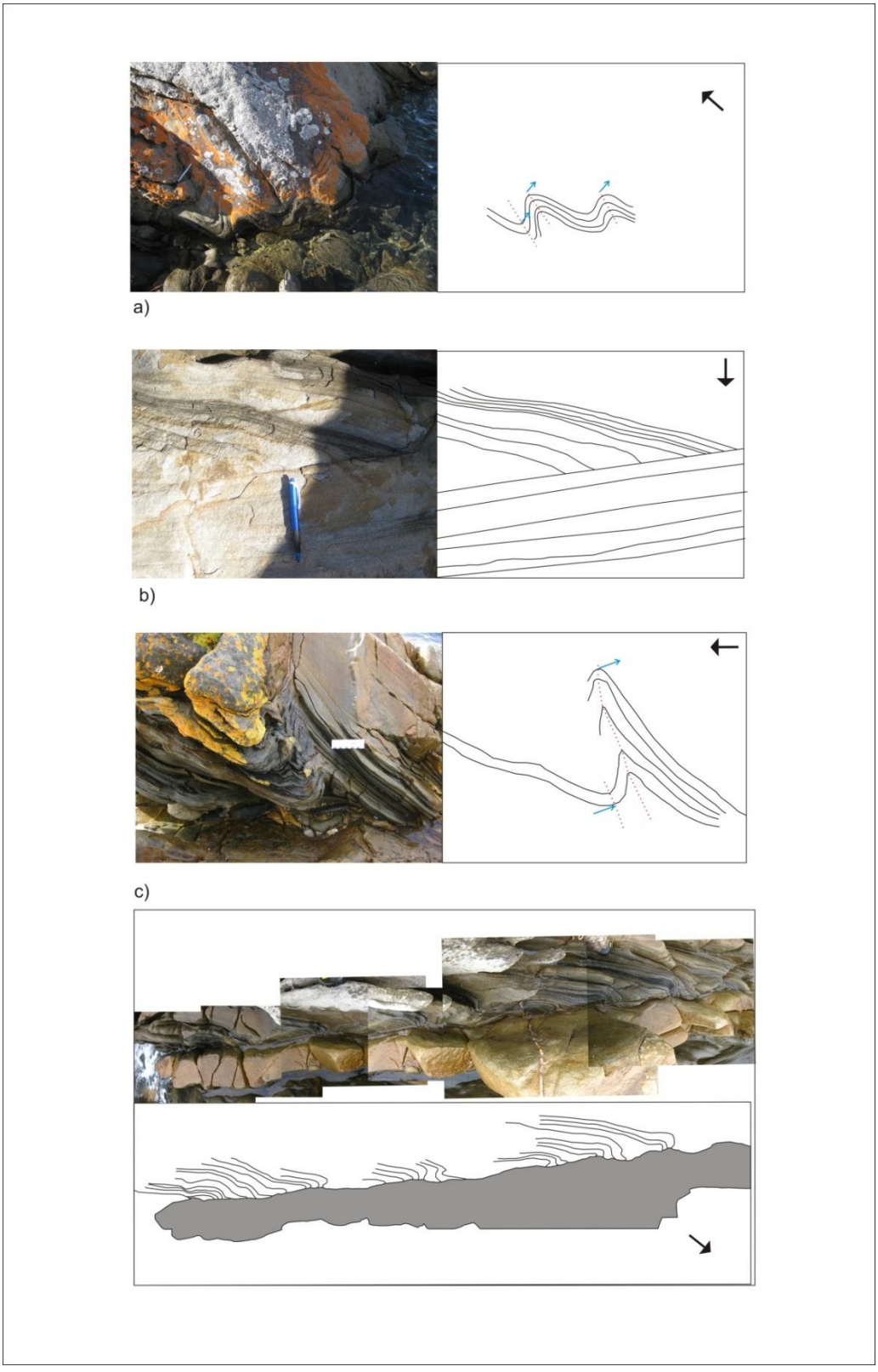

Figure 12

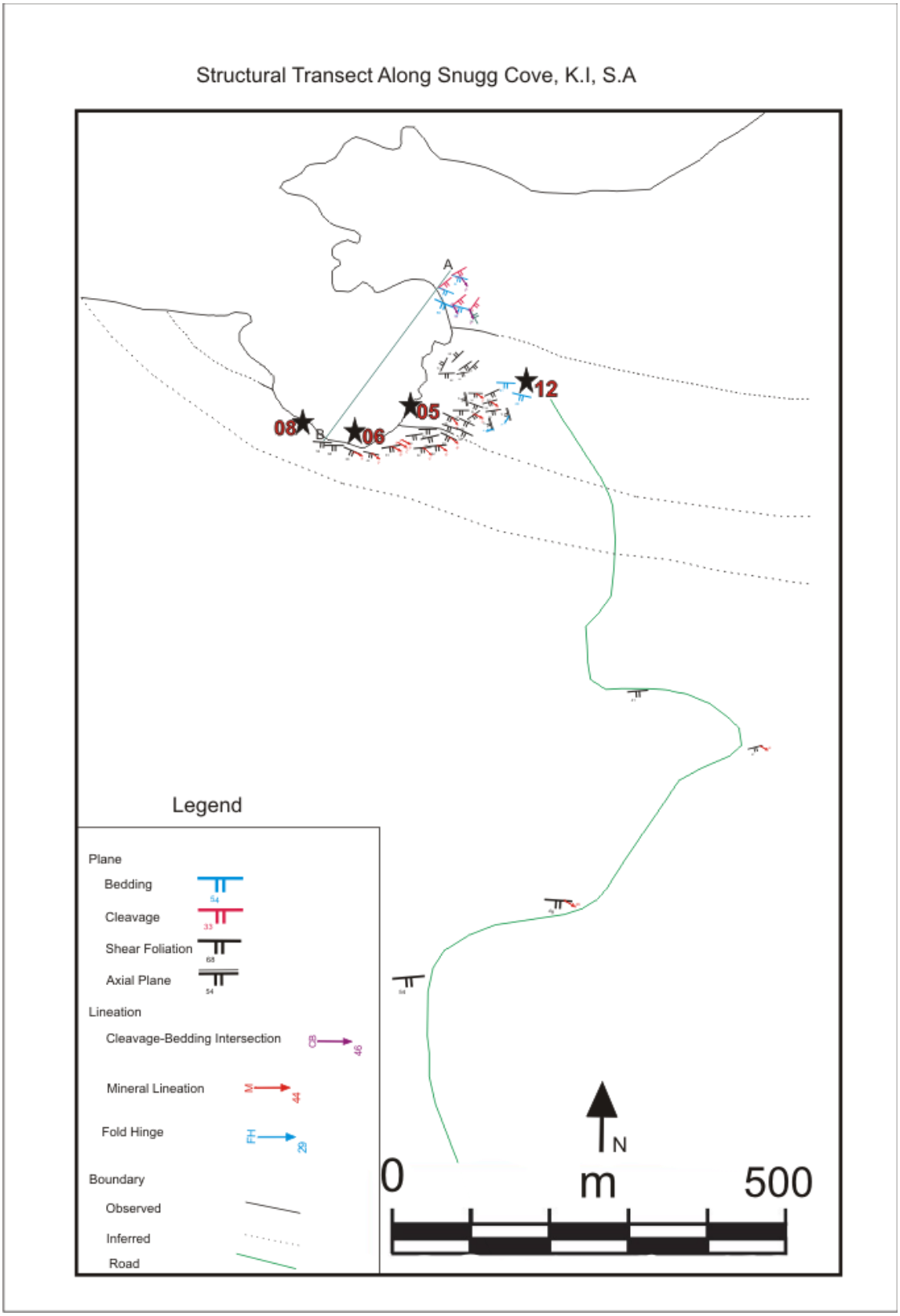
Structural Transect Along Snugg Cove, K.I, S.A
A
B
08
06
05
12
Legend
Plane
Bedding
Cleavage
Shear Foliation
Axial Plane
Lineation
Cleavage-Bedding Intersection
Mineral Lineation
Fold Hinge
Boundary
Observed
Inferred
Road
N
0
m
500

Figure 13

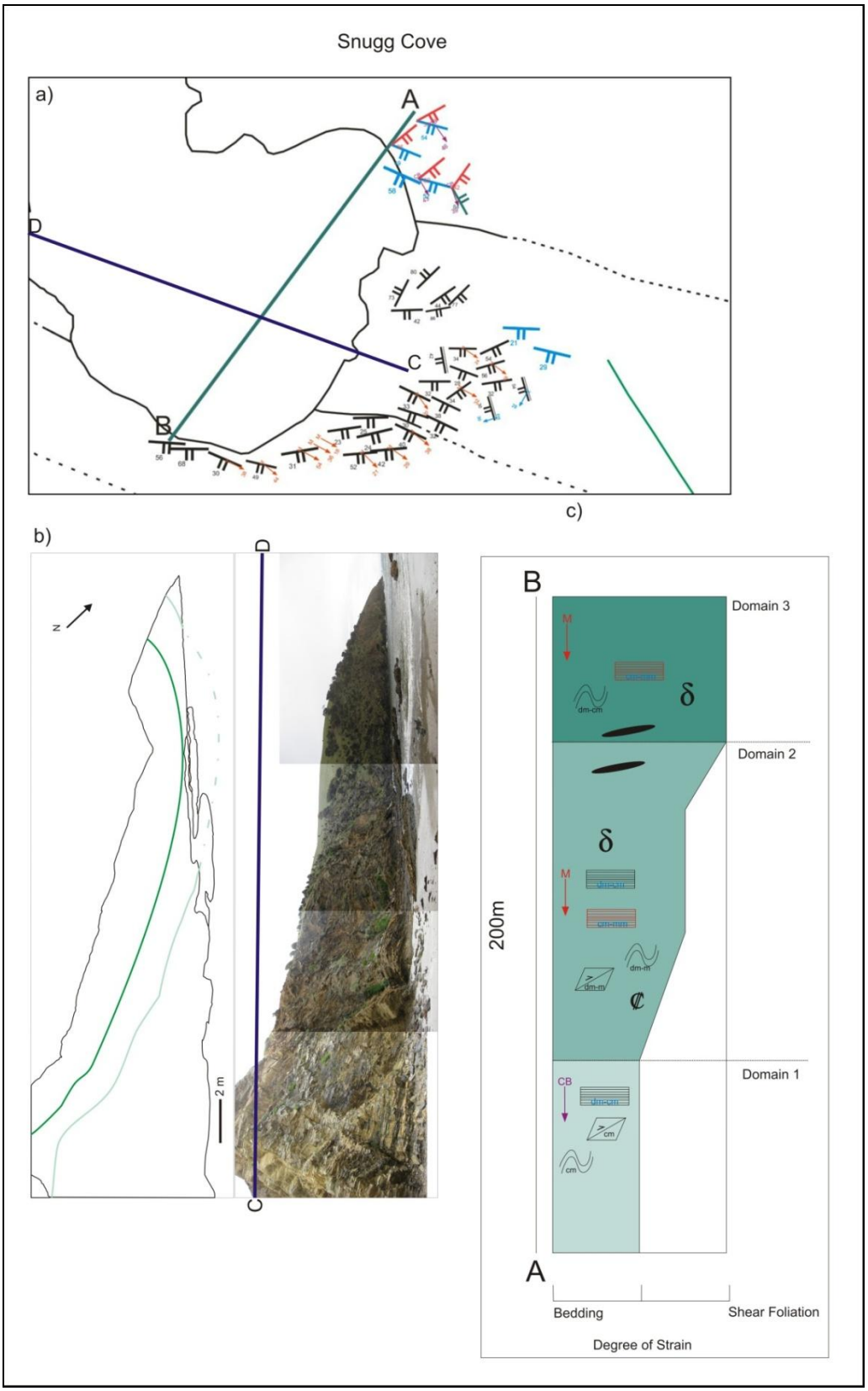
Snugg Cove
a)
A
D
C
B
c)
b)
D
N
2 m
C
B
Domain 3
M
δ
dm-cm
Domain 2
δ
M
dm-m
dm-m
Domain 1
CB
cm
cm
200m
A
Bedding
Shear Foliation
Degree of Strain

Figure 14

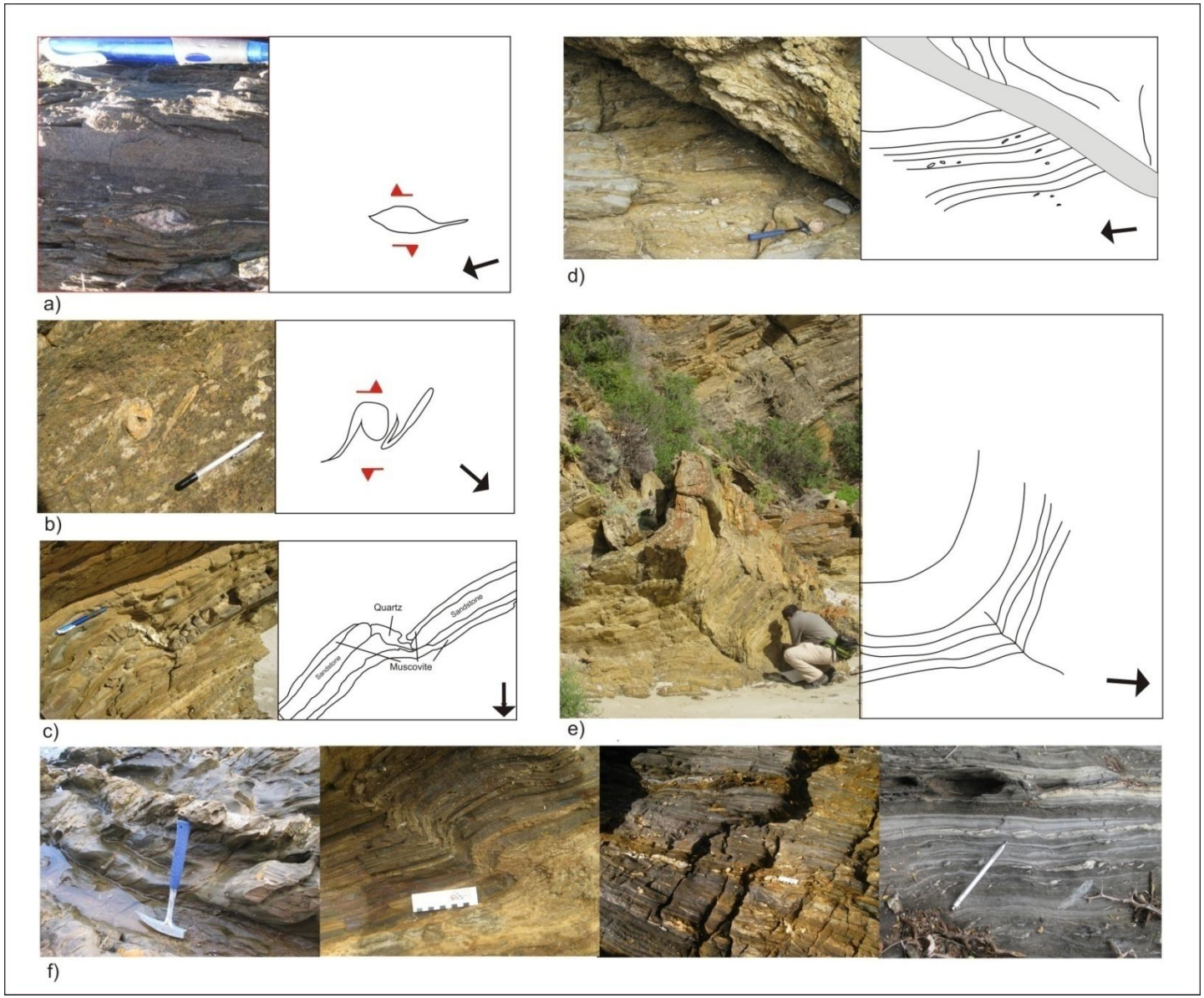

Figure 15

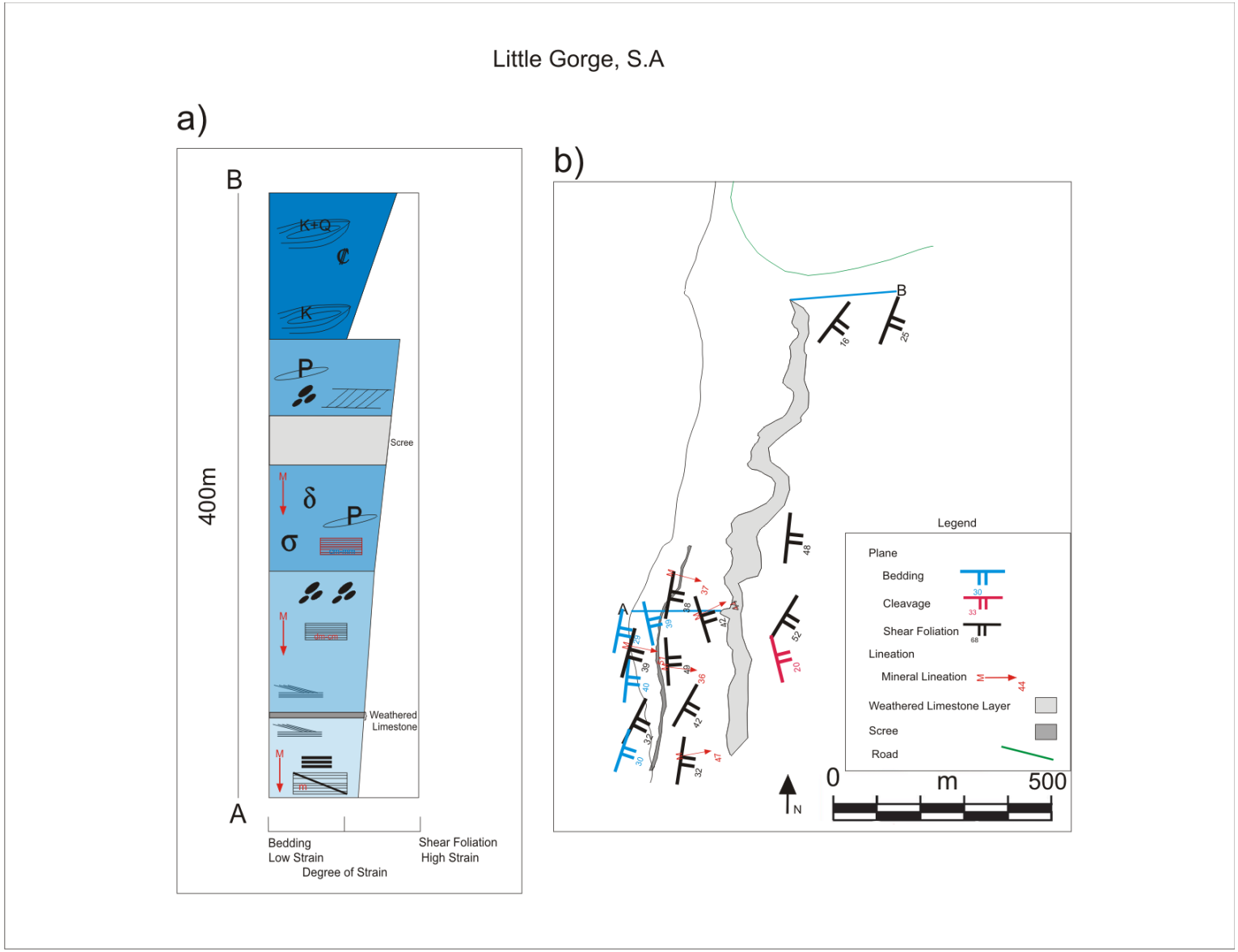
Little Gorge, S.A
a)
B
A
400m
K+Q
K
P
Scree
δ
σ
Weathered
Limestone
Bedding
Low Strain
Shear Foliation
High Strain
Degree of Strain
b)
B
A
Legend
Plane
Bedding
Cleavage
Shear Foliation
Lineation
Mineral Lineation
Weathered Limestone Layer
Scree
Road
0
m
500
N

Figure 16

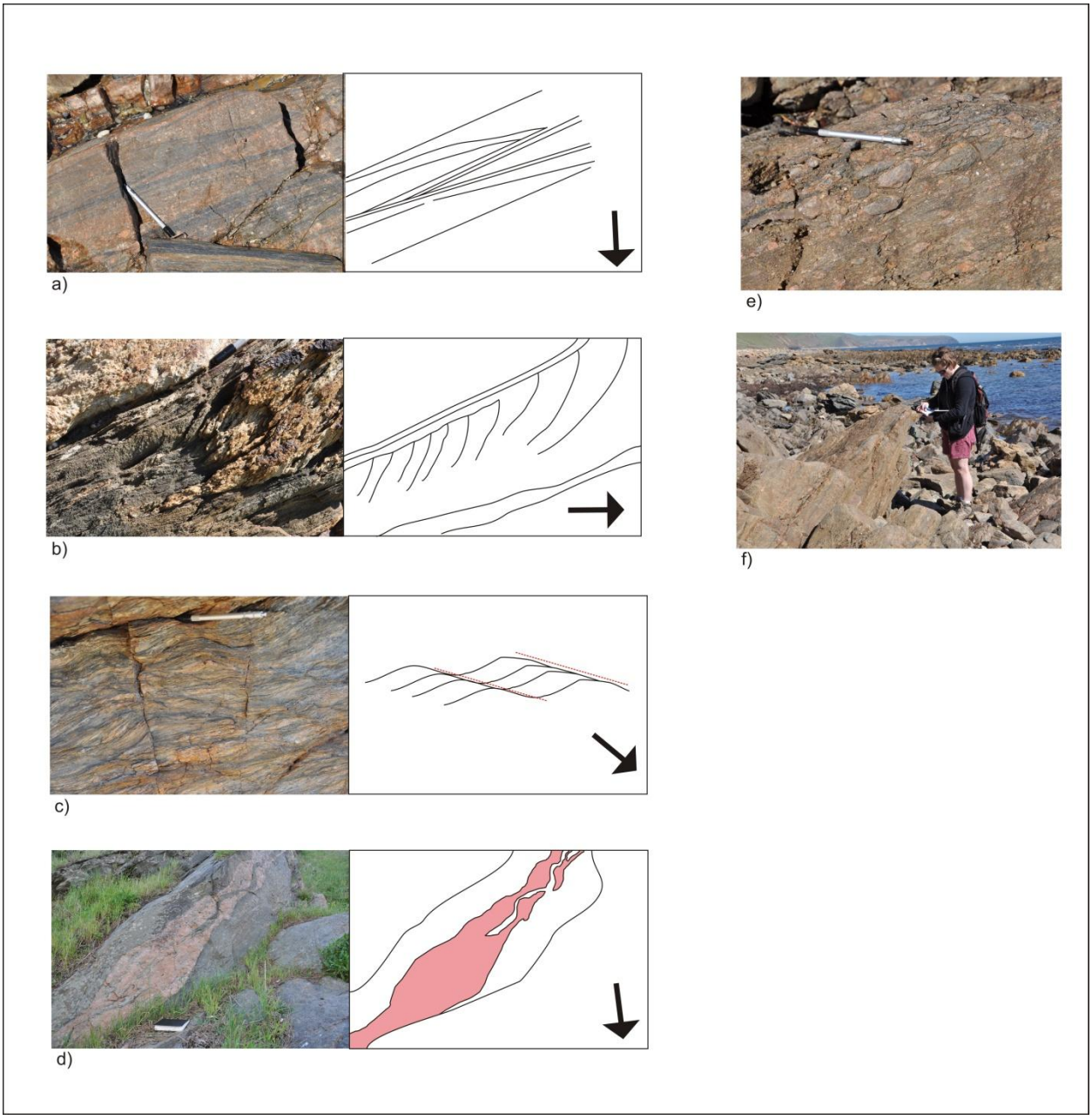

Figure 17

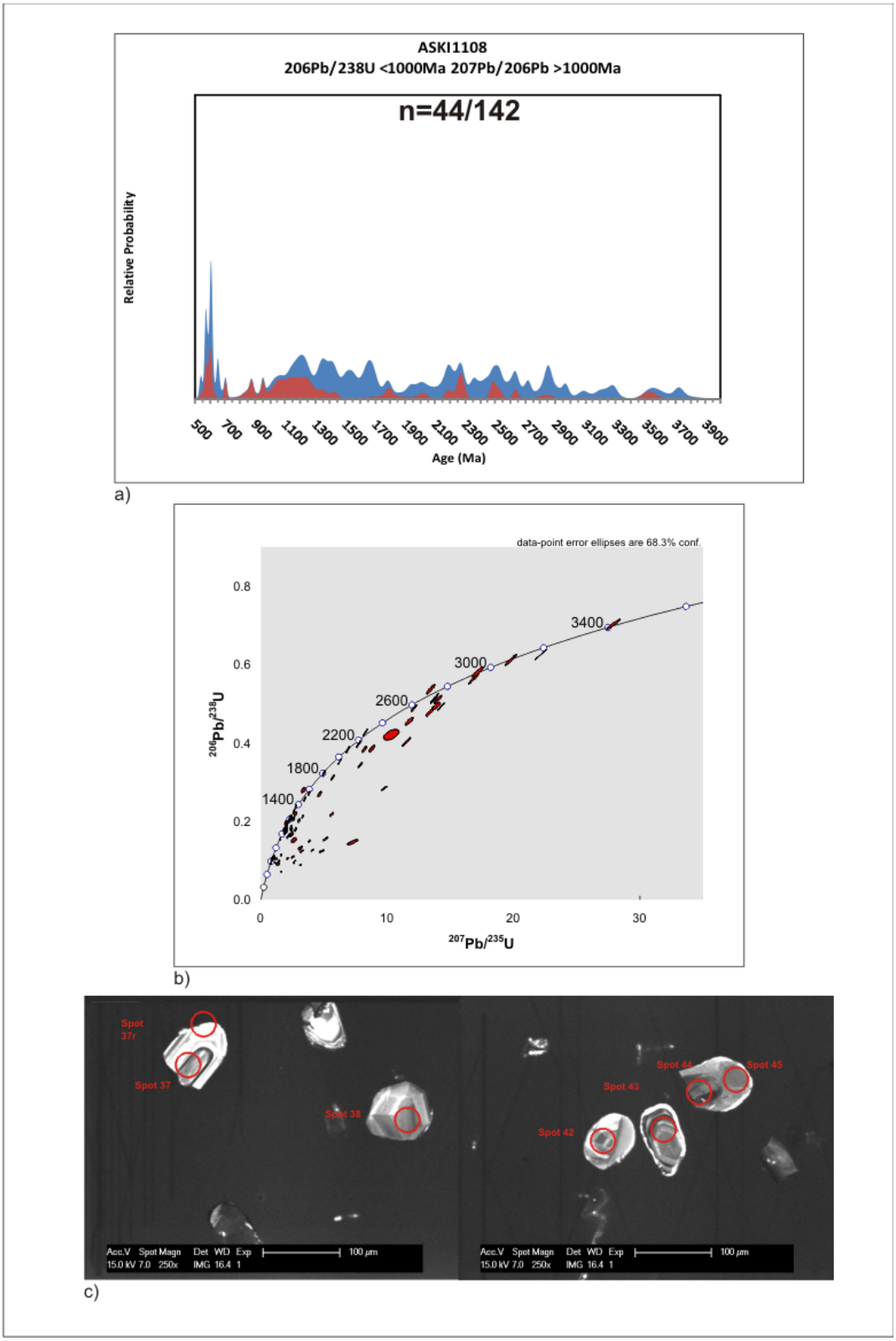
ASKI1108
206Pb/238U <1000Ma 207Pb/206Pb >1000Ma
n=44/142
Relative Probability
500 700 900 1100 1300 1500 1700 1900 2100 2300 2500 2700 2900 3100 3300 3500 3700 3900
Age (Ma)
a)
data-point error ellipses are 68.3% conf.
0.8
0.6
0.4
0.2
0.0
206Pb/238U
3400
3000
2600
2200
1800
1400
0
10
20
30
207Pb/235U
b)
Spot 37r
Spot 37
Spot 38
Spot 44
Spot 45
Spot 43
Spot 42
Acc.V Spot Magn Det WD Exp 100 µm
15.0 kV 7.0 250x IMG 16.4 1
c)

Figure 18

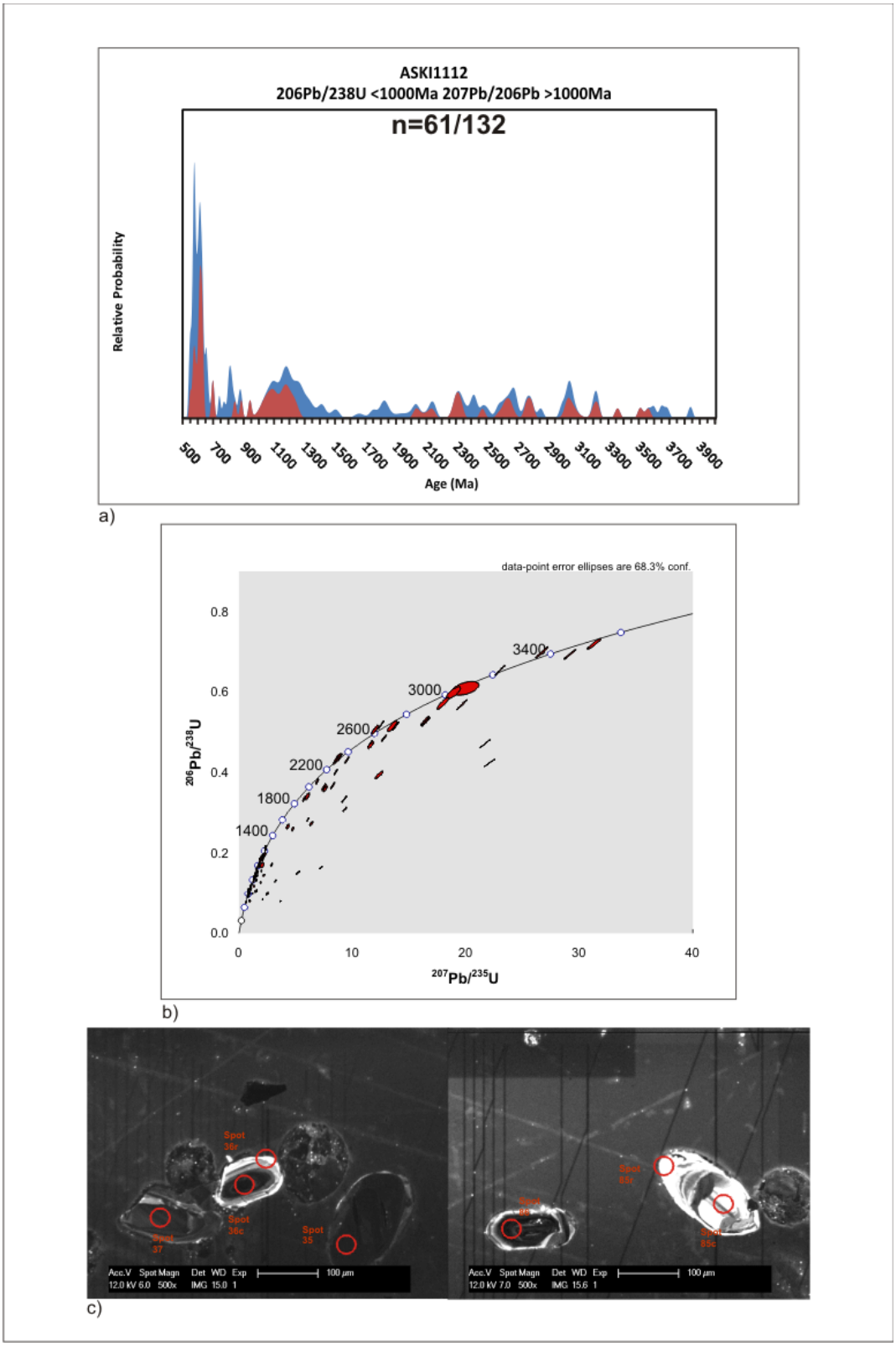
ASKI1112
206Pb/238U <1000Ma 207Pb/206Pb >1000Ma
n=61/132
Relative Probability
500 700 900 1100 1300 1500 1700 1900 2100 2300 2500 2700 2900 3100 3300 3500 3700 3900
Age (Ma)
a)
data-point error ellipses are 68.3% conf.
0.8
0.6
0.4
0.2
0.0
206Pb/238U
3400
3000
2600
2200
1800
1400
0
10
20
30
40
207Pb/235U
b)
Spot 36r
Spot 36c
Spot 37
Spot 35
Acc.V Spot Magn Det WD Exp 100 µm
12.0 kV 6.0 500x IMG 15.0 1
Spot 85r
Spot 85c
Acc.V Spot Magn Det WD Exp 100 µm
12.0 kV 7.0 500x IMG 15.6 1
c)

Figure 19

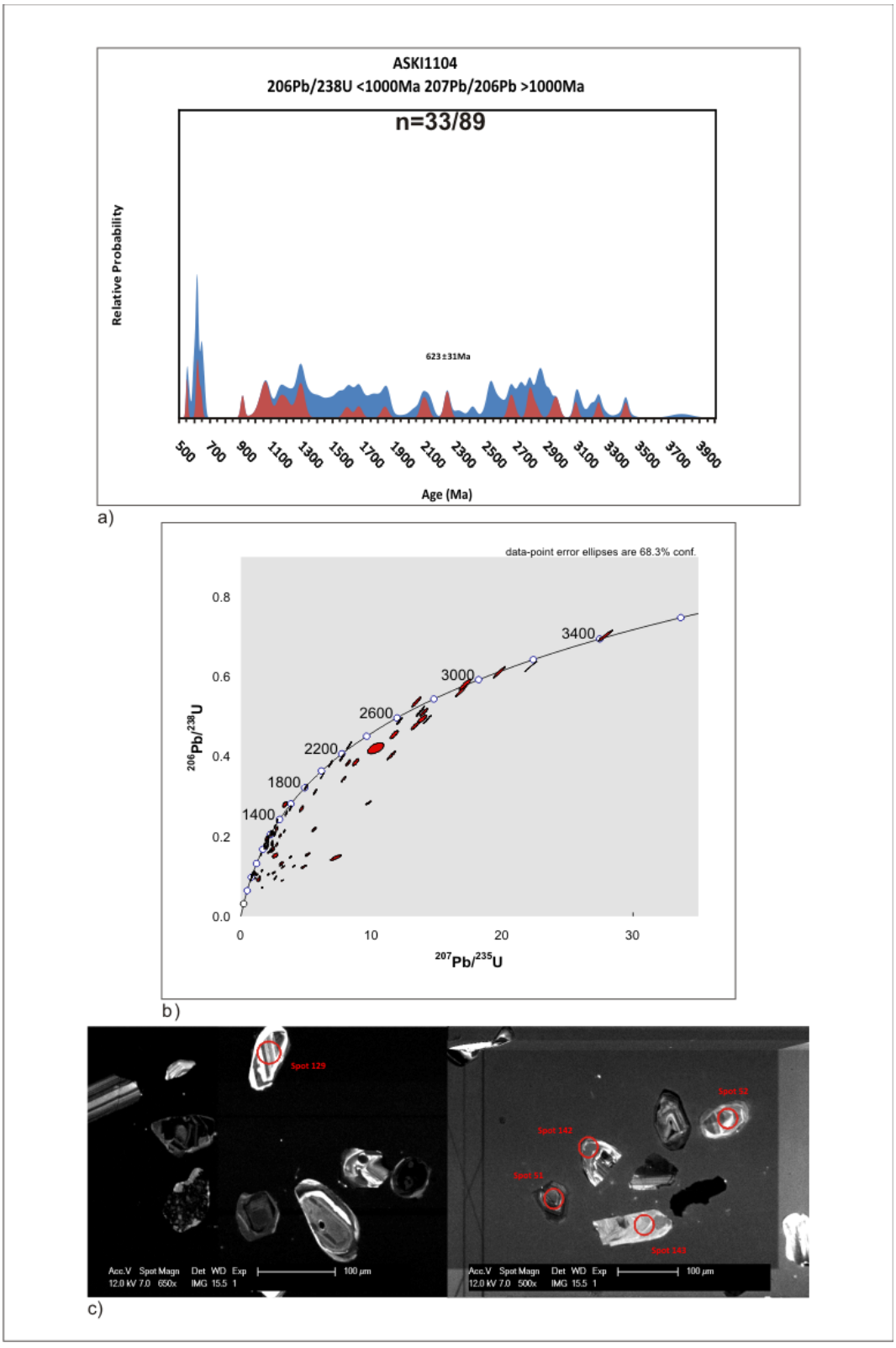
ASKI1104
206Pb/238U <1000Ma 207Pb/206Pb >1000Ma
n=33/89
Relative Probability
623±31Ma
500 700 900 1100 1300 1500 1700 1900 2100 2300 2500 2700 2900 3100 3300 3500 3700 3900
Age (Ma)
a)
data-point error ellipses are 68.3% conf.
0.8
0.6
0.4
0.2
0.0
206Pb/238U
3400
3000
2600
2200
1800
1400
0
10
20
30
207Pb/235U
b)
Spot 129
Spot 52
Spot 142
Spot 51
Spot 143
Acc.V Spot Magn Det WD Exp 100 µm
12.0 kV 7.0 650x IMG 15.5 1
Acc.V Spot Magn Det WD Exp 100 µm
12.0 kV 7.0 500x IMG 15.5 1
c)

Figure 20

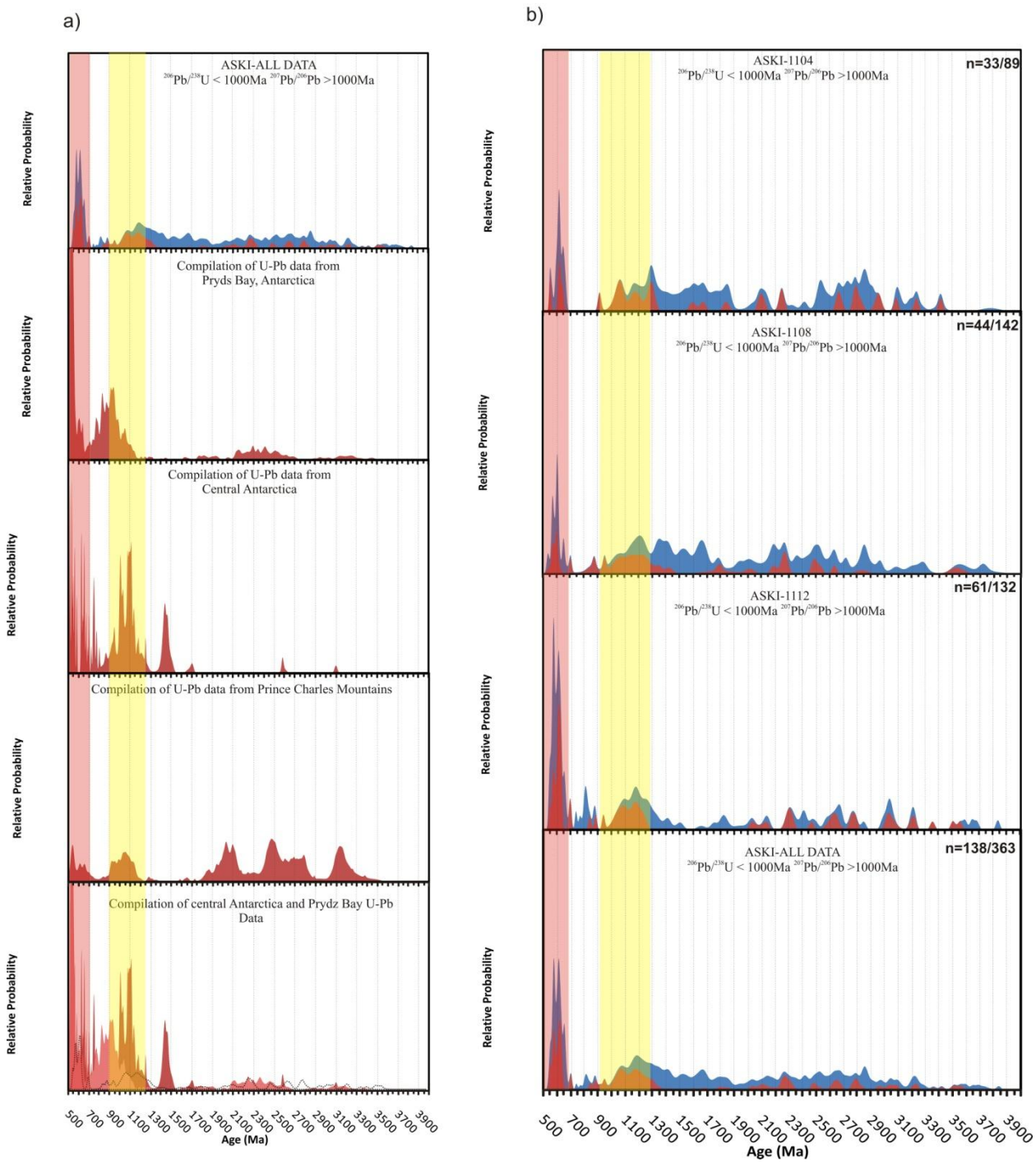
a)
ASKI-ALL DATA
206Pb/238U < 1000Ma 207Pb/206Pb >1000Ma
Compilation of U-Pb data from Pryds Bay, Antarctica
Compilation of U-Pb data from Central Antarctica
Compilation of U-Pb data from Prince Charles Mountains
Compilation of central Antarctica and Prydz Bay U-Pb Data
Relative Probability
500 700 900 1100 1300 1500 1700 1900 2100 2300 2500 2700 2900 3100 3300 3500 3700 3900
Age (Ma)
b)
ASKI-1104
206Pb/238U < 1000Ma 207Pb/206Pb >1000Ma
n=33/89
ASKI-1108
206Pb/238U < 1000Ma 207Pb/206Pb >1000Ma
n=44/142
ASKI-1112
206Pb/238U < 1000Ma 207Pb/206Pb >1000Ma
n=61/132
ASKI-ALL DATA
206Pb/238U < 1000Ma 207Pb/206Pb >1000Ma
n=138/363
Relative Probability
500 700 900 1100 1300 1500 1700 1900 2100 2300 2500 2700 2900 3100 3300 3500 3700 3900
Age (Ma)

Figure 21

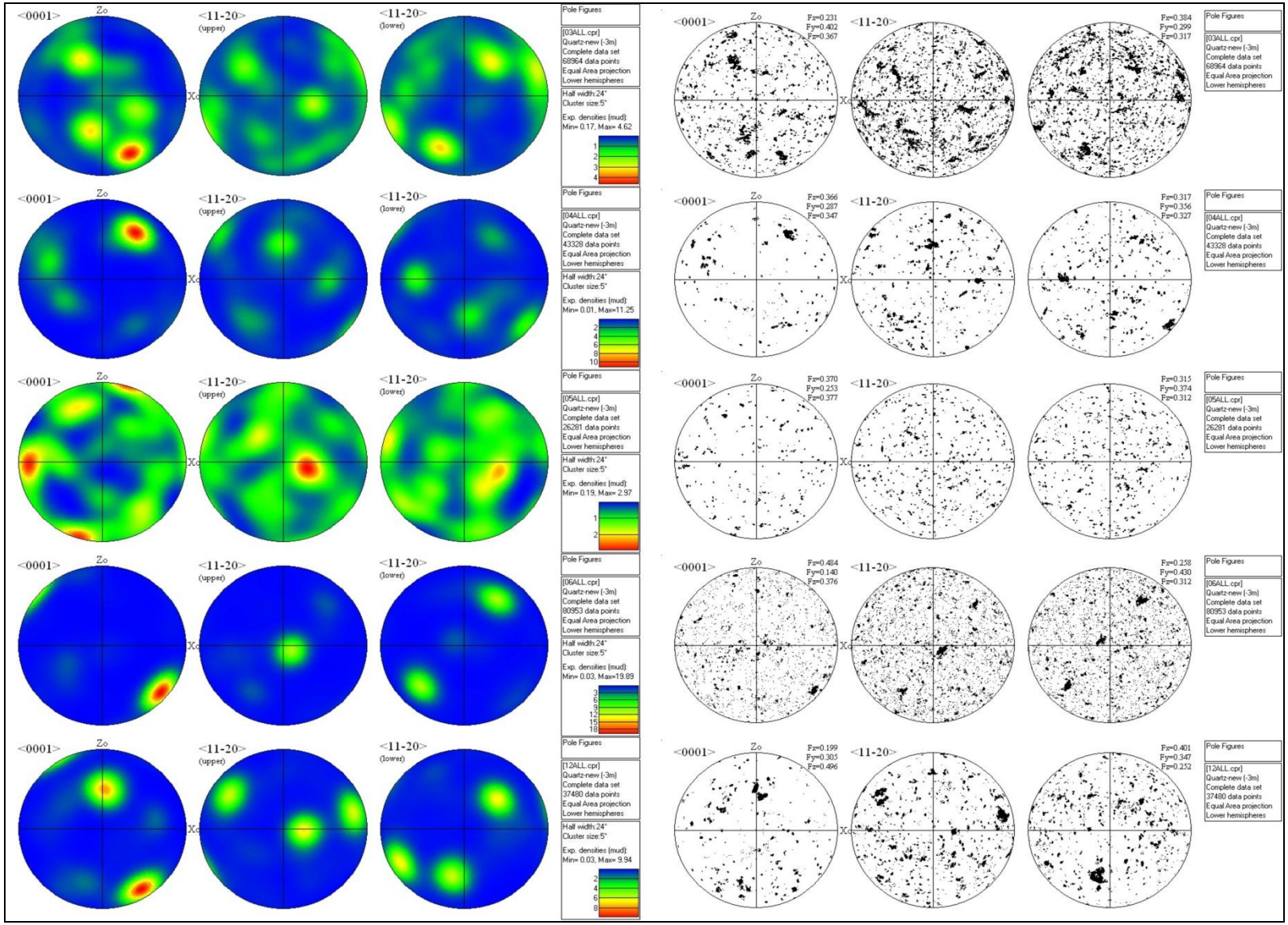
<0001>
Zo
<11-20>
(upper)
<11-20>
(lower)
Xo
Pole Figures
[03ALL.cpr]
Quartz-new (-3m)
Complete data set
68964 data points
Equal Area projection
Lower hemispheres
Half width:24°
Cluster size:5°
Exp. densities (mud):
Min= 0.17, Max= 4.62
1
2
3
4
Fx=0.231
Fy=0.402
Fz=0.367
Fx=0.384
Fy=0.299
Fz=0.317
[04ALL.cpr]
43328 data points
Min= 0.01, Max=11.25
2
4
6
8
10
Fx=0.366
Fy=0.287
Fz=0.347
Fx=0.317
Fy=0.356
Fz=0.327
[05ALL.cpr]
26281 data points
Min= 0.19, Max= 2.97
1
2
Fx=0.370
Fy=0.253
Fz=0.377
Fx=0.315
Fy=0.374
Fz=0.312
[06ALL.cpr]
80953 data points
Min= 0.03, Max=19.89
3
6
9
12
15
18
Fx=0.424
Fy=0.140
Fz=0.376
Fx=0.258
Fy=0.430
Fz=0.312
[12ALL.cpr]
37480 data points
Min= 0.03, Max= 9.94
2
4
6
8
Fx=0.199
Fy=0.305
Fz=0.496
Fx=0.401
Fy=0.347
Fz=0.252

Figure 22

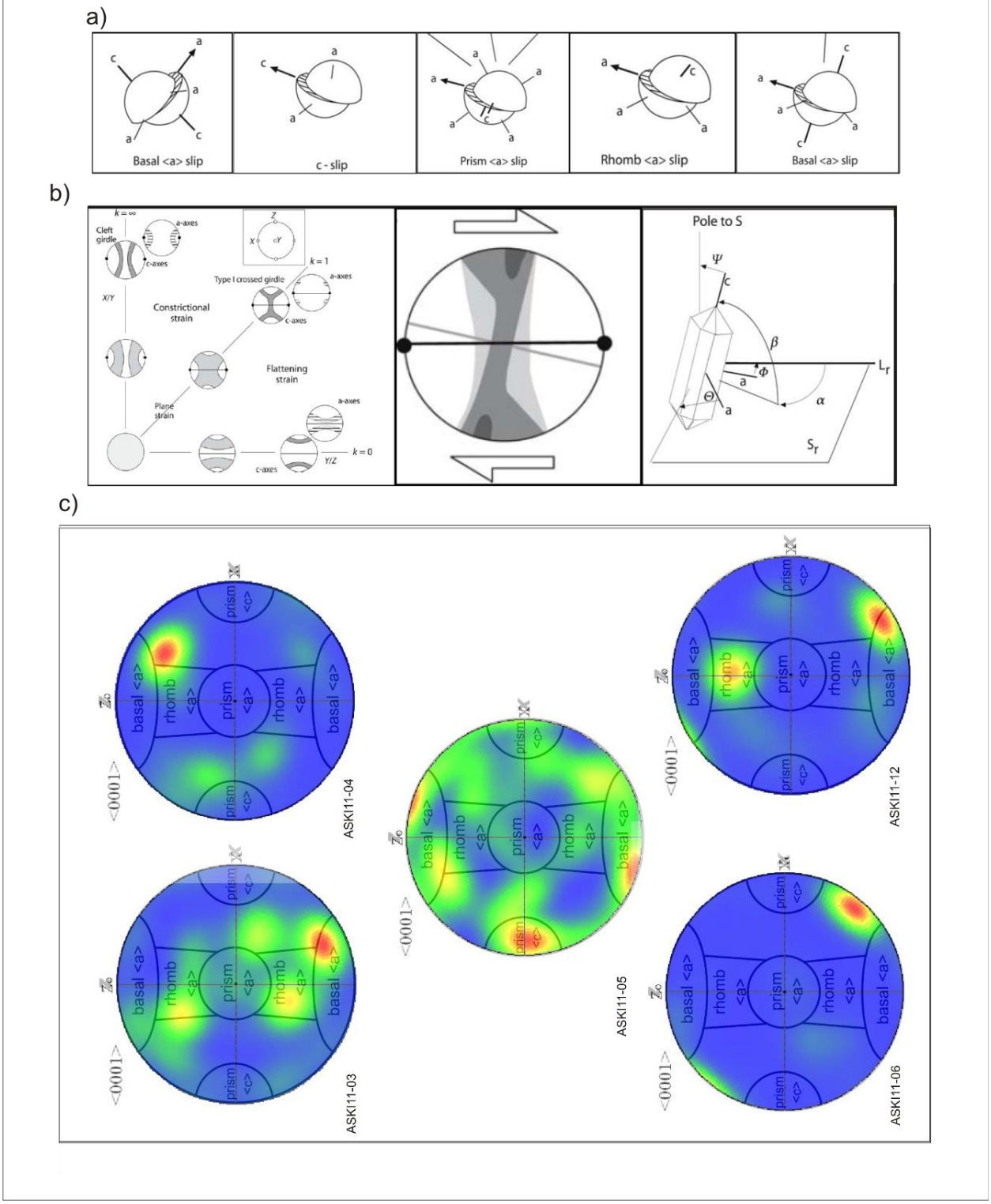
a)
Basal <a> slip
c - slip
Prism <a> slip
Rhomb <a> slip
Basal <a> slip
b)
Cleft girdle
a-axes
c-axes
Type I crossed girdle
Constrictional strain
Flattening strain
Plane strain
Pole to S
c)
ASKI11-04
ASKI11-12
ASKI11-03
ASKI11-05
ASKI11-06
basal <a>
rhomb <a>
prism <a>
prism <c>
<0001>

Figure 23

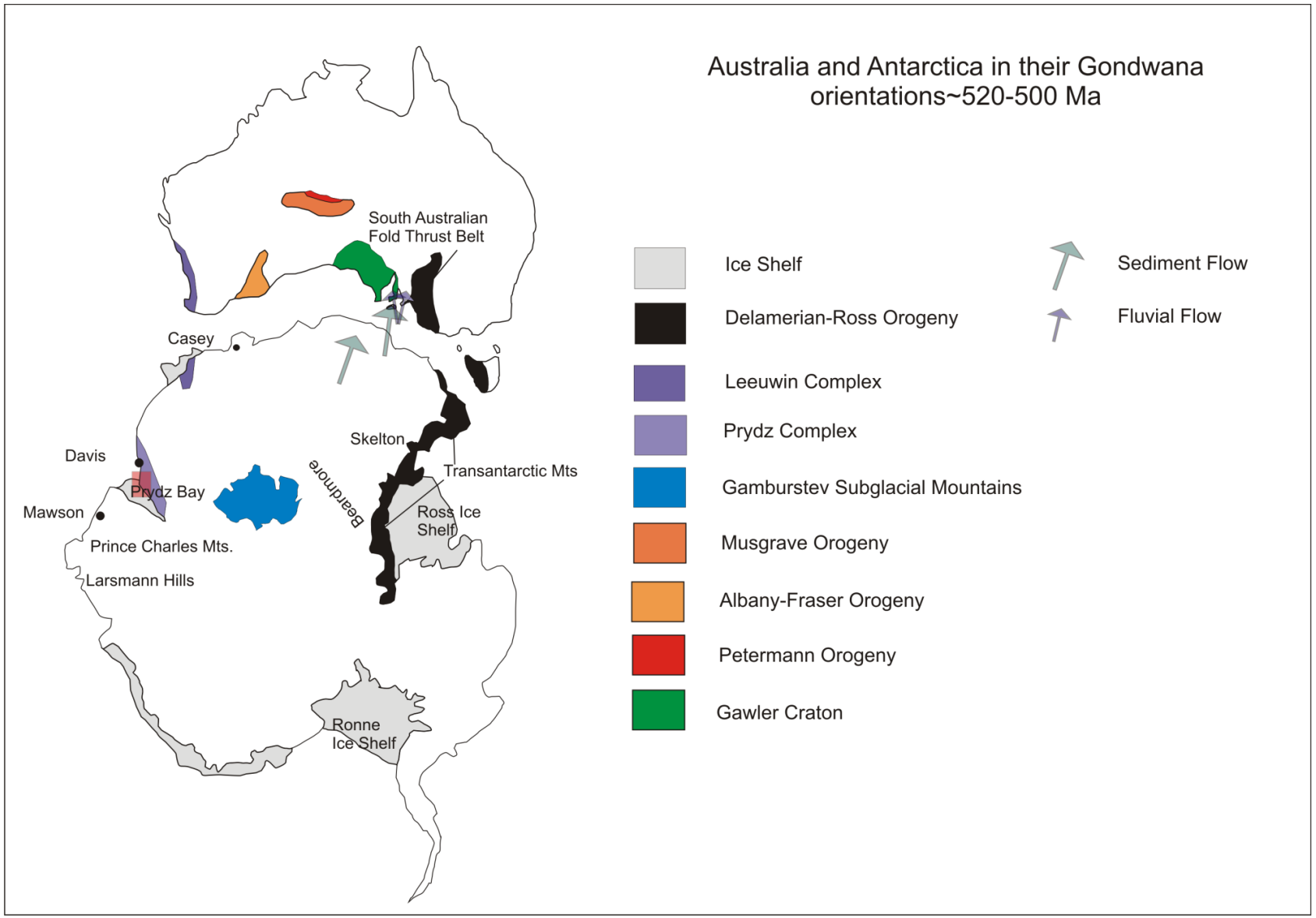
Australia and Antarctica in their Gondwana orientations~520-500 Ma
South Australian Fold Thrust Belt
Casey
Davis
Prydz Bay
Mawson
Prince Charles Mts.
Larsmann Hills
Skelton
Transantarctic Mts
Beardmore
Ross Ice Shelf
Ronne Ice Shelf
Ice Shelf
Delamerian-Ross Orogeny
Leeuwin Complex
Prydz Complex
Gamburstev Subglacial Mountains
Musgrave Orogeny
Albany-Fraser Orogeny
Petermann Orogeny
Gawler Craton
Sediment Flow
Fluvial Flow

Figure 24

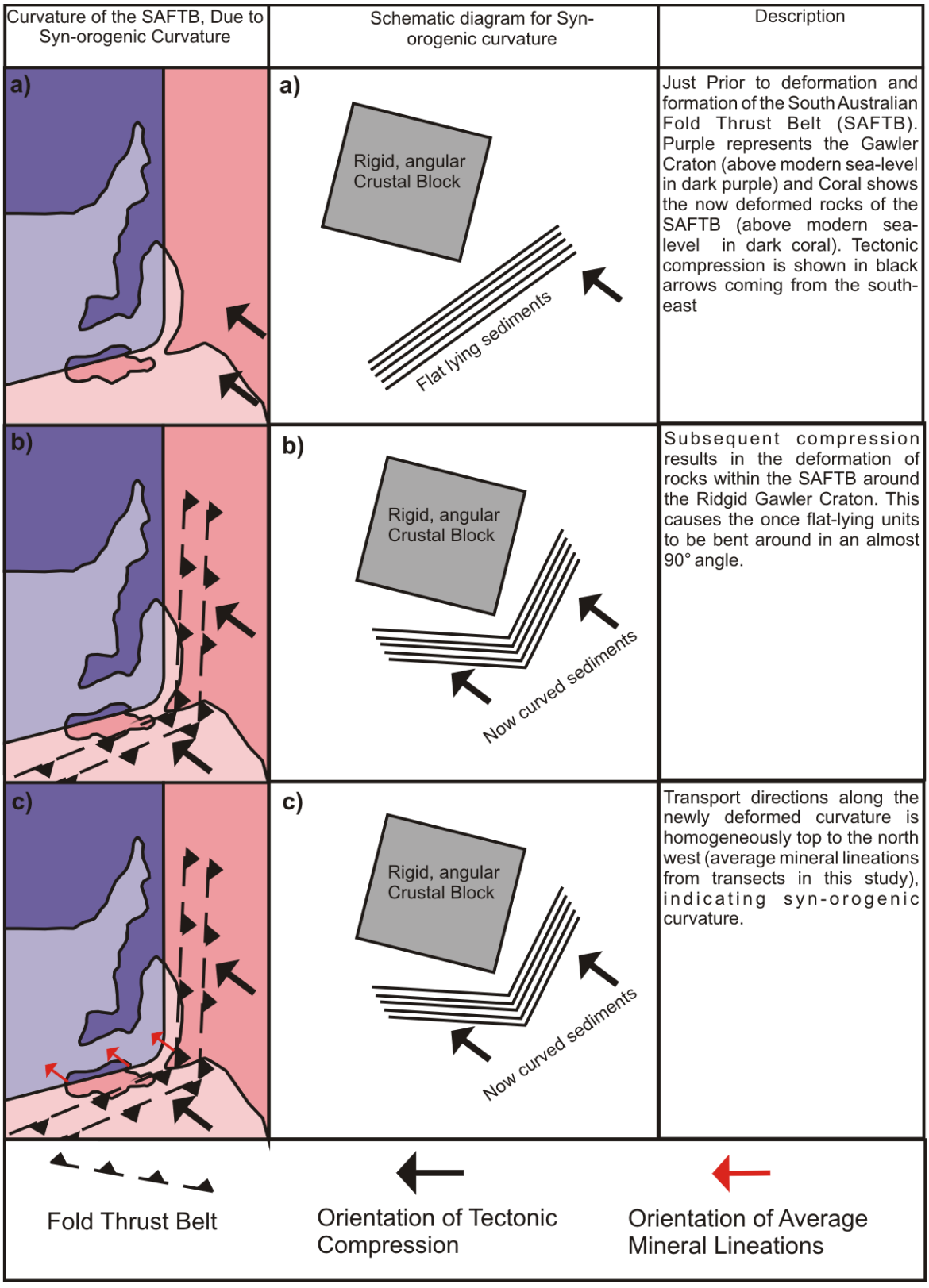
Curvature of the SAFTB, Due to Syn-orogenic Curvature
Schematic diagram for Syn-orogenic curvature
Description
a)
a)
Rigid, angular Crustal Block
Flat lying sediments
Just Prior to deformation and formation of the South Australian Fold Thrust Belt (SAFTB). Purple represents the Gawler Craton (above modern sea-level in dark purple) and Coral shows the now deformed rocks of the SAFTB (above modern sea-level in dark coral). Tectonic compression is shown in black arrows coming from the south-east
b)
b)
Rigid, angular Crustal Block
Now curved sediments
Subsequent compression results in the deformation of rocks within the SAFTB around the Ridgid Gawler Craton. This causes the once flat-lying units to be bent around in an almost 90° angle.
c)
c)
Rigid, angular Crustal Block
Now curved sediments
Transport directions along the newly deformed curvature is homogeneously top to the north west (average mineral lineations from transects in this study), indicating syn-orogenic curvature.
Fold Thrust Belt
Orientation of Tectonic Compression
Orientation of Average Mineral Lineations

Figure 25

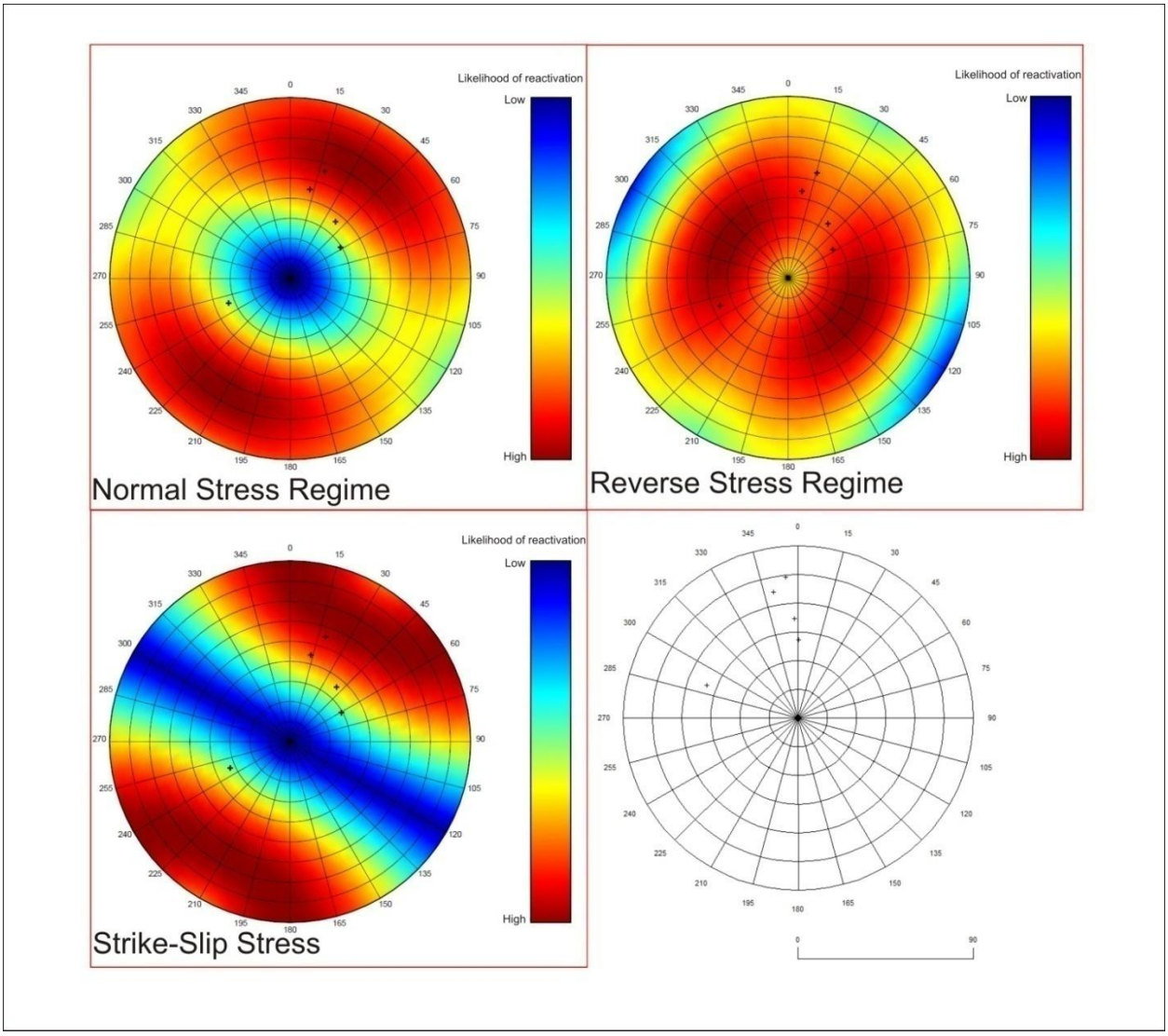
Likelihood of reactivation
Low
High
Normal Stress Regime
Likelihood of reactivation
Low
High
Reverse Stress Regime
Likelihood of reactivation
Low
High
Strike-Slip Stress
0
90

Figure 26

APPENDICES

Appendix 1 Methods

Appendix 2 U-Pb zircon tables

See attachments